

# Emerging Ultralow-Temperature Electrolytes for Lithium Batteries Operated Below $-30^{\circ}\text{C}$

Wanyao Zhang, Tao Teng, Weiyu Wang, Wenyu Kuang, Di Lu, Xianxian Shi, Yufang Chen, Chunman Zheng,\* Jilei Liu, and Peitao Xiao\*

Lithium batteries operated at  $\leq -30^{\circ}\text{C}$  have been attracted overwhelming attentions, while encountering severe challenges, especially charging at temperatures below  $-30^{\circ}\text{C}$ , one of which is how to design ideal low-temperature electrolytes. In low-temperature lithium batteries, electrolytes play a crucial role in the transport of  $\text{Li}^{+}$ , maintaining the stability of the electrode-electrolyte interface and enhancing the batteries' kinetics. Herein, we comprehensively summarize recent strategies for designing low-temperature

electrolytes, elucidating how lithium salts, solvents, and additives regulate the solvation structure of  $\text{Li}^{+}$ , stabilize the interface, and influence electrochemical performance at low-temperature. Moreover, prospects are provided for the design and commercialization of low-temperature electrolytes in this review. Different from previous reviews, we mainly focused on low-temperature electrolytes for lithium batteries operated at  $\leq -30^{\circ}\text{C}$ , especially for those can still charge at  $\leq -30^{\circ}\text{C}$ .

## 1. Introduction

Nowadays, new-generation defense equipment, including aerospace aircraft and equipment used in polar/deep-sea exploration, lunar exploration program, and deep space exploration, are experiencing rapid development.<sup>[1,2]</sup> As a critical component of these systems, batteries are confronted with increasingly severe challenges in these harsh environments. Since the 1990s, lithium-ion batteries (LIBs) have dominated the market due to their excellent cycle stability and energy density.<sup>[3–5]</sup> However, their performance deteriorates rapidly at ultralow-temperature ( $\leq -30^{\circ}\text{C}$ ), making it difficult to meet the requirements for extreme conditions.<sup>[6,7]</sup> Therefore, there is an urgent need to develop novel lithium batteries with high energy density and exceptional stability at low-temperature.

At low-temperature, lithium batteries encounter a multitude of challenges in practical applications. These challenges include increased electrolyte viscosity, diminished ion conductivity, sluggish ion desolvation processes, elevated interfacial impedance, lithium dendrite/lithium plating, and significantly decreased ion diffusion rates within electrode materials.<sup>[8–15]</sup> To overcome

these limitations and improve the low-temperature performance of LIBs, the most effective strategies are to develop or modify high-performance cathodes, anodes, and electrolytes.<sup>[16–22]</sup>

As an essential medium for  $\text{Li}^{+}$  transport, electrolytes are crucial for stabilizing the electrode-electrolyte interface and enhancing the kinetics of LIBs.<sup>[23–26]</sup> On the one hand, stable electrode-electrolyte interfaces (EEIs, including solid electrolyte interface, SEI, and cathode-electrolyte interface, CEI) can effectively suppress the formation of lithium dendrites at low-temperature, reduces side reactions between lithium metal and the electrolyte, alleviates the increase in interfacial impedance, and suppresses the phase transition and pulverization processes of cathode, thereby significantly enhancing the electrochemical performance of LIBs.<sup>[27–32]</sup> On the other hand, electrolytes with low viscosity and a wide liquid phase range can reduce the transport barriers of  $\text{Li}^{+}$  at low-temperature, thereby improving the cycle life and dynamic performance of lithium batteries.<sup>[33]</sup> However, ethylene carbonate (EC), an indispensable component in commercial electrolytes, has a high melting point ( $36.4^{\circ}\text{C}$ ) and high viscosity, leading to electrolyte solidification at low-temperature, hindering ions transport.<sup>[34–41]</sup> Therefore, it is urgent to design novel low-temperature electrolytes to meet the performance requirements of LIBs at low-temperature.

The main components of the electrolyte in LIBs are lithium salts, solvents, and functional additives. With the decrease of temperature, especially at  $<30^{\circ}\text{C}$ , the solvation structures of  $\text{Li}^{+}$  in the traditional electrolytes undergoes essential remodeling compared with those at room temperature, and the solvation structures of  $\text{Li}^{+}$  and its desolvation directly determines ionic conductivity, charge transfer resistance, and interfacial resistance, all of which significantly affect the electrochemical kinetics, especially at low temperatures. Compared with the solvation structures dominated by solvent separation ion pairs (SSIP) at room temperature, the coordination number of solvent molecules in the first solvation shell increases with decreasing the temperatures, making it much more

W. Zhang, T. Teng, W. Wang, W. Kuang, D. Lu, X. Shi, Y. Chen, C. Zheng,  
P. Xiao

College of Aerospace Science and Engineering  
National University of Defense Technology  
Changsha, Hunan 410073, China  
E-mail: zhengchunman@nudt.edu.cn  
xiaopt@nudt.edu.cn

J. Liu  
College of Materials Science and Engineering  
Hunan Joint International Laboratory of Advanced Materials and  
Technology of Clean Energy  
Hunan Province Key Laboratory for Advanced Carbon Materials and  
Applied Technology  
Hunan University Changsha  
Changsha, Hunan 410082, China

difficult for  $\text{Li}^+$  to detach from the solvation sheath, and the desolvation process becomes the decisive step in the electrochemical process. By designing and optimizing the electrolyte components, researchers have made great progress in improving the temperature adaptability and the corresponding performance of LIBs.<sup>[1]</sup> For example, the adoption of weak solvating solvents makes it easier for anions to replace solvent molecules into the primary solvation sheath, promoting the transformation of solvation structure from SSIP to contact ion pair (CIP) or aggregated ion pair (AGG), forming an anion-dominated solvation structure, which not only affects the electric double layer and leading to anion-derived electrode-electrolyte interphases but also alleviates the desolvation process, thus resulting into enhanced low-temperature performance.

Previous reviews focused on LIBs with wide operating temperature ranges. In this review, we will summarize the recent development of strategies to design and optimize low-temperature electrolyte for LIBs at  $\leq -30^\circ\text{C}$ , especially charging at  $\leq -30^\circ\text{C}$ . Specifically, the key effects of lithium salts, solvents, and additives on regulating the solvation structure, film forming capacity, and the electrochemical performances are emphasized (Figure 1).

## 2. Lithium Salts

The most commonly used lithium salts in electrolytes include lithium hexafluorophosphate ( $\text{LiPF}_6$ ), lithium bis(fluorosulfonyl)imide ( $\text{LiFSI}$ ), lithium bis(trifluoromethanesulfonyl)imide ( $\text{LiTFSI}$ ), lithium tetrafluoroborate ( $\text{LiBF}_4$ ), and lithium bis(oxalate)borate ( $\text{LiBOB}$ ), lithium oxalatodifluoroborate ( $\text{LiODFB}$ ).<sup>[42,43]</sup> In addition, researchers have been persistently exploring new lithium salts, with the goal of regulating solvation structures and optimizing the composition/structure of the EEIs to extend the operational temperature range of electrolytes.<sup>[44–48]</sup>

For example, Xu et al. investigated how anion solvation influenced the electrochemical performance of electrolytes. They developed a novel lithium salt with an asymmetric anion, (fluorosulfonyl)(trifluoromethanesulfonyl) imide (FTFSI), and dissolved the lithium salt in a weakly solvating solvent, bis(3-fluoropropyl) ether (BFPE). Results of *in situ* liquid secondary ion mass spectrometry and molecular modeling showed that FTFSI anion strongly interacted with BFPE (Figure 2a,b). As a result,  $\text{Li}||\text{LiNi}_{0.8}\text{Co}_{0.1}\text{Mn}_{0.1}\text{O}_2$  (NCM811) cells using 1.5 M LiTFSI-BFPE



Figure 1. Schematic illustration of the contents in the review.

electrolyte retained 63% of their room-temperature capacity even at  $-40^\circ\text{C}$ .<sup>[49]</sup> Similarly, Li et al. explored the potential of lithium difluorophosphate ( $\text{LiPO}_2\text{F}_2$ ) in dimethyl carbonate (DMC)/ethyl methyl carbonate (EMC) to enhance the electrochemical performance (1 M  $\text{LiPF}_6$  in DMC/EMC (3:5 w/w) + 4vol% PC + 0.2vol% FEC + 2wt%  $\text{LiPO}_2\text{F}_2$ ). Addition of  $\text{LiPO}_2\text{F}_2$  facilitated the formation of a thicker and more uniform CEI on the particle surface (Figure 2c,d), which effectively prevented the coininsertion of solvated  $\text{Li}^+$ , thereby stabilizing the cathode and improving its overall performance.<sup>[50]</sup> Consequently,  $\text{LiPO}_2\text{F}_2$  not only enhanced the low-temperature electrochemical performance of the cells by participating in CEI film formation but also inhibited further decomposition of the electrolyte, contributing to the overall cycling stability, so that  $\text{Li}||\text{NCM811}$  cells still had a discharge capacity of  $81.97 \text{ mAh g}^{-1}$  after 50 cycles at  $-40^\circ\text{C}$ .

Double-salt regulation strategies have also been explored for low-temperature LIBs. For instance, Zhao et al. reported a strategy involving a strong solvent with dual lithium salts. Dimethyl sulfite (DMS) solvent, which has a high dielectric constant, strong polarity, and low melting point, was adopted to dissolve LiFSI to provide high ionic conductivity. Additionally, the weak dissociation of LiODFB promoted  $\text{Li}^+$  desolvation by manipulating the solvation structure (Figure 2e). By balancing the relationship between dissolution and desolvation through the dual-salt system, Graphite (Gr)||  $\text{Li}_2\text{CO}_3$  (LCO) cells achieved a wide operating



**Chunman Zheng** obtained his BS and PhD degrees from the National University of Defense Technology in 2000 and 2006, respectively. Then, he joined the faculty of the National University of Defense Technology in 2007. He was a visiting scholar at the University of St. Andrew in 2012 and is currently a head professor of material science and engineering. Professor Zheng's current research interests include new electrode materials, high-performance energy storage devices, power supplies, and systems for extreme environments.



**Peitao Xiao** received his BS degree and MS degree from Tianjin University in 2010 and 2013, respectively, and his PhD degree from Fudan University in 2019. Then, he worked as a research engineer at Envision AESC and a postdoc fellow at Tsinghua University. Now, he is an assistant professor at the National University of Defense Technology. His research interests include advanced batteries with high energy density at ultralow/high temperatures and advanced electrolytes/electrodes via AI.

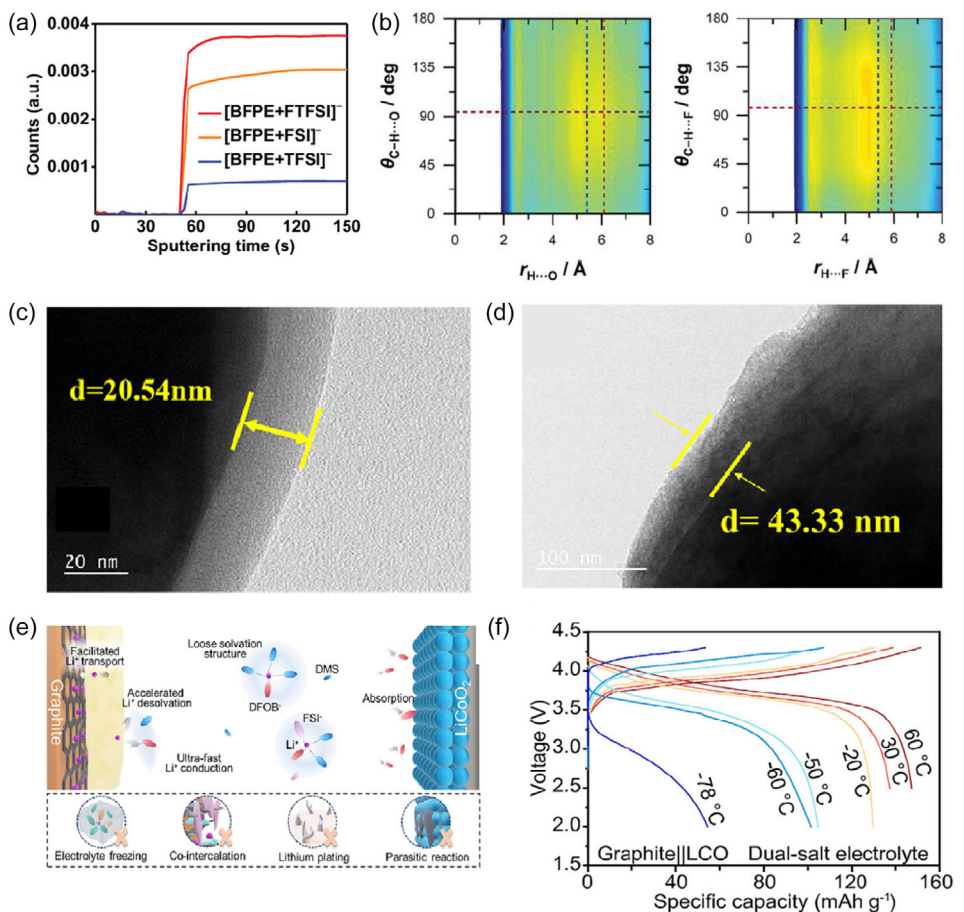


**Figure 2.** a) Depth profiles of 0.5 M LiFSI + 0.5 M LiFTFSI + 0.5 M LiTFSI in BFPE electrolytes under the negative ion mode. Reproduced with permission.<sup>[49]</sup> Copyright 2023, Wiley. b) The molecular simulation of the ion-molecule interaction between solvent molecules with H···F and C-H···O atomic pairs of BFPE and FTFSI<sup>-</sup> and the corresponding H bond angles C-H···F and C-H···O. Reproduced with permission.<sup>[49]</sup> Copyright 2023, Wiley. TEM images of cycled NCM811 cathodes with 2 wt% LiPO<sub>2</sub>F<sub>2</sub>; c) at room temperature after 100 cycles and d) at -40 °C after 50 cycles. Reproduced with permission.<sup>[50]</sup> Copyright 2022, American Chemical Society. e) Schematic diagram of the dual salts electrolyte and the limitations faced by mainstream low-temperature electrolyte. Reproduced with permission.<sup>[51]</sup> Copyright 2023 American Chemical Society. f) Discharge curves of Gr||LCO cells using dual-salt electrolyte under 60 °C (3 C), 30 °C (3 C), -20 °C (0.2 C), -50 °C (0.05 C), -60 °C (0.02 C), and -78 °C (0.01 C). Reproduced with permission.<sup>[51]</sup> Copyright 2023, American Chemical Society.

temperature range from -78 to 60 °C (Figure 2f).<sup>[51]</sup> Meng et al. also used LiFSI as the primary salt and LiODFB as the auxiliary salt in their electrolyte. The combination of LiFSI and LiODFB significantly mitigated the corrosion of aluminum foil induced by LiFSI (Figure 3a). By carefully tuning the ratio of the dual salts and incorporating lithium nitrate (LiNO<sub>3</sub>) as an additive, anion-rich composition within the solvation structure was obtained, which successfully broadened the electrochemical window of the electrolyte, optimized the lithium deposition morphology, and enabled Li||LiNi<sub>0.5</sub>Co<sub>0.2</sub>Mn<sub>0.3</sub>O<sub>2</sub> (NCM523) full cells to achieve stable 150 charge-discharge cycles at -40 °C (Figure 3b).<sup>[52]</sup> Che et al. successfully enhanced the compatibility of the Ethyl acetate (EA)-based electrolyte with Gr anodes by leveraging the synergistic effects of anions. Specifically, the ODFB<sup>-</sup>, characterized by its low solvation number, was incorporated into the solvation sheath layer, significantly reducing the desolvation energy of Li<sup>+</sup>. Moreover, the reduction of these two anions (ODFB<sup>-</sup> and FSI<sup>-</sup>) facilitated the formation of an inorganic-rich SEI, thereby

enhancing the stability of the electrode-electrolyte interface (Figure 3c). As a result, LiFePO<sub>4</sub> (LFP) ||Gr pouch cells demonstrated remarkable thermal stability, retaining 66.28% of its room-temperature capacity even at -40 °C.<sup>[53]</sup> In the further exploration of dual salt regulation strategy, Zhao et al. incorporated two lithium salts, namely LiNO<sub>3</sub> and LiPO<sub>2</sub>F<sub>2</sub>, into the diglyme (G2) solvent. The anions in these salts both possess high binding energies with Li<sup>+</sup> and small ionic radii, enabling them to easily penetrate the primary solvation sheath. As a result, the coordination between the solvent and Li<sup>+</sup> is significantly weakened. This reduction in coordination strength, in turn, lowers the desolvation energy of Li<sup>+</sup> and improves the rate performance of the battery (Figure 3d). Consequently, Li||NCM811 cells achieve a remarkable capacity retention of 91.2% after 150 cycles at -30 °C with a cut-off voltage of 4.4 V (Figure 3e).<sup>[54]</sup>

Cheng et al. successfully developed a highly chaotic electrolyte system by introducing lithium trifluoride, which significantly enhanced the entropy of the electrolyte while achieving an

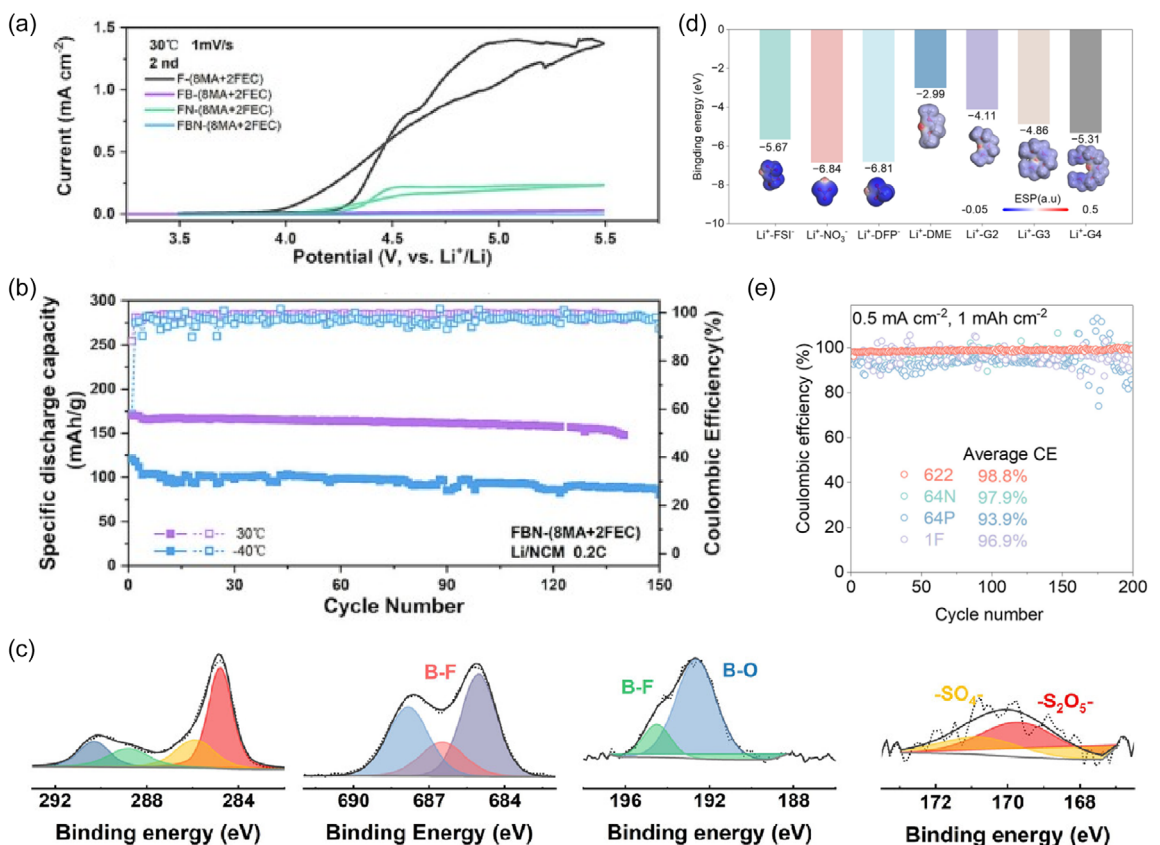


**Figure 3.** a) CV curves of Li||Al cells using different electrolytes. Reproduced with permission.<sup>[52]</sup> Copyright 2023, Elsevier. b) Cycling performance of Li||NCM523 cells at 30 and -40 °C. Reproduced with permission.<sup>[52]</sup> Copyright 2023, Elsevier. c) X-ray photoelectron spectroscopy spectra of the solid electrolyte interphase on the Gr anode. Reproduced with permission.<sup>[53]</sup> Copyright 2024, Wiley. d) The binding energy and electrostatic potential of the Li<sup>+</sup>-solvent/anion complex. Reproduced with permission.<sup>[54]</sup> Copyright 2025, KeAi. e) CE curves of Li||Cu cells at 0.5, 1.0 mAh cm<sup>-2</sup> within different electrolyte. Reproduced with permission.<sup>[54]</sup> Copyright 2025, KeAi.

anion-rich solvation structure and weak solvation interactions. This formed in a stable F-rich interface, rapid desolvation, and diffusion kinetics, enabling high-voltage performance and wide-temperature adaptability in lithium metal batteries (Figure 4a). Consequently, the Li||NCM811 cells utilizing this highly chaotic electrolyte demonstrated remarkable performance, maintaining a capacity retention of 73% after 200 cycles under stringent conditions of -30 °C with a ultrahigh cut-off voltage of 4.7 V (Figure 4b).<sup>[55]</sup>

Inspired by the concept of high-entropy alloys, researchers have introduced multiple components to increase the configurational entropy, thus designing high-entropy electrolytes. In high-entropy electrolytes, the configurational entropy increases with the number of components introduced, thus leading to a decrease in Gibbs free energy (Figure 4c). For electrolytes with a low fraction of lithium salts, solubility is primarily determined by the mixing enthalpy change ( $\Delta H_{\text{mix}}$ ), as shown in the following equation

$$\Delta G_{\text{mix}} = \Delta H_{\text{mix}} - T\Delta S_{\text{mix}} \quad (1)$$

When  $\Delta H_{\text{mix}}$  is negative, the solubility of lithium salts decreases with decrease of  $\Delta H_{\text{mix}}$ , potentially leading to

precipitation beyond the solubility limit at a given temperature and pressure. By introducing multiple components to increase the mixing entropy change ( $\Delta S_{\text{mix}}$ ), the solubility of specific salts can be enhanced to some extent. Meanwhile, introduction of various lithium salts increases the entropy, thereby lowering the freezing point and expanding the working temperature range of the electrolyte without altering the solvents (Figure 4d).

Based on this principle, Wang et al. designed a high entropy electrolyte consisting of 0.15 M LiPF<sub>6</sub>, 0.15 M LiFSI, 0.15 M LiTFSI, 0.15 M LiODFB, and 0.15 M LiNO<sub>3</sub>, in a mixture of propylene carbonate (PC) and diethyl carbonate (DEC) (1:1 w/w), with 5% fluoroethylene carbonate (FEC) as additive. Compared with single-salt electrolytes, high-entropy electrolytes significantly enhance the solubility of LiNO<sub>3</sub> by several orders (Figure 4e). This improvement of solubility is attributed to the altered solvation structure and interactions between the solvent and anion groups, which in turn lead to higher conductivity, transference number of Li<sup>+</sup>, and exchange current density (Figure 4f). These results further demonstrate that increasing entropy effectively improves bulk Li<sup>+</sup> transport and charge transfer processes. Consequently, the capacity retention of Li||NCM811 cells with high entropy electrolytes exceeds 99% at -20 °C, and the Coulomb efficiency (CE) of Li||Cu cells remain above 80% at -40 °C (Figure 4g).<sup>[56]</sup>

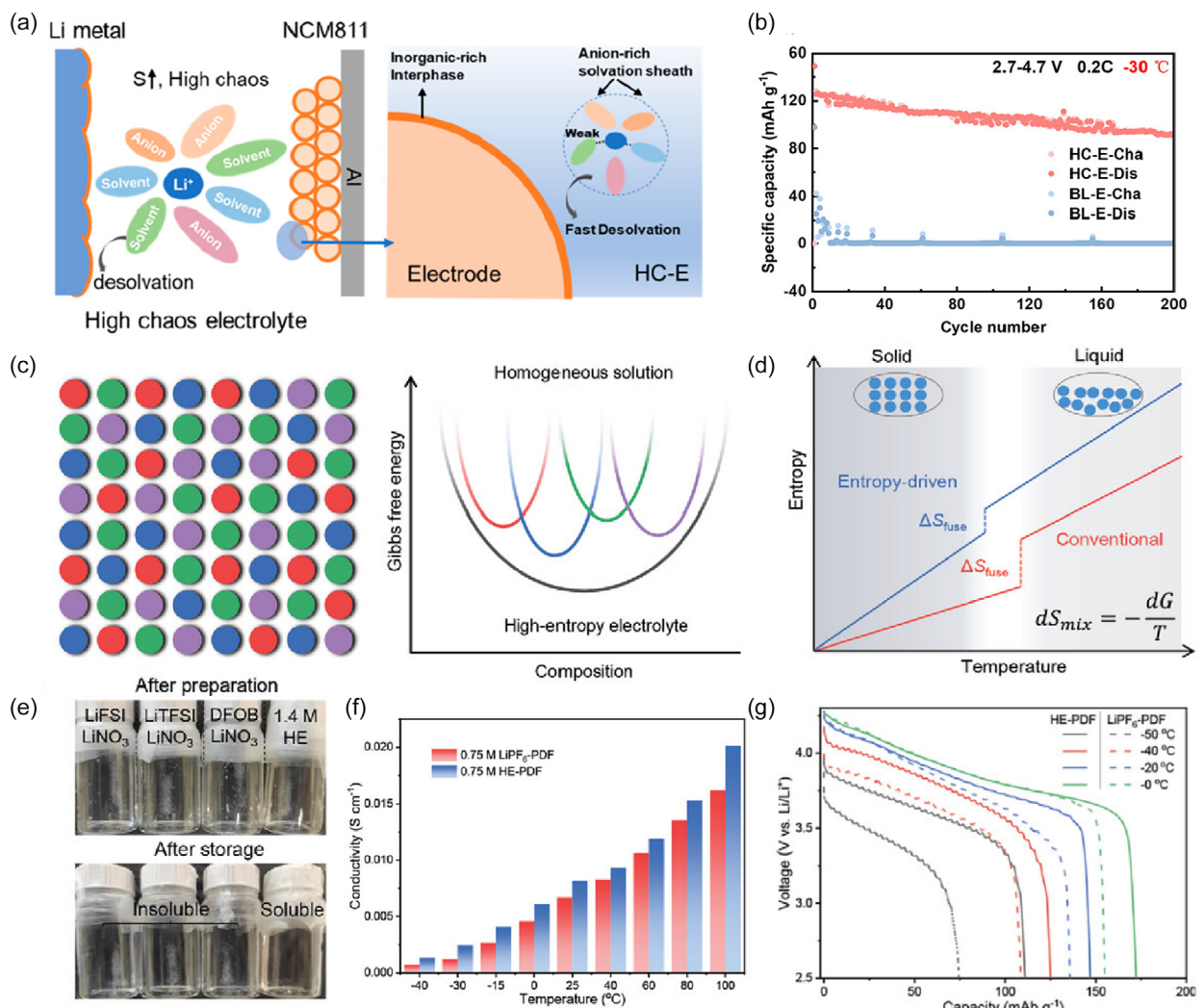


**Figure 4.** a) Conceptual diagram of chaos enhanced design. S stands for entropy. Reproduced with permission.<sup>[55]</sup> Copyright 2023, American Chemical Society. b) Cycling performance of NCM811||Li cells with different electrolytes at -30 °C. Reproduced with permission.<sup>[55]</sup> Copyright 2023 American Chemical Society. c) Schematic diagram of the composition structure and energy of a uniform solution with increased mixing entropy by mixing multiple components. Reproduced with permission.<sup>[56]</sup> Copyright 2023 Wiley. d) Solubility of different salts in EC/DMC (weight ratio 1:1) and 5% FEC. Reproduced with permission.<sup>[56]</sup> Copyright 2023 Wiley. e) Ionic conductivity of the 0.75 M LiPF<sub>6</sub>-PDF and 0.75 M HE-PDF electrolytes at -40 ≈ 100 °C. Reproduced with permission.<sup>[56]</sup> Copyright 2023 Wiley. f) Schematic diagram of entropy variation with temperature during phase transition. Reproduced with permission.<sup>[56]</sup> Copyright 2023 Wiley. g) Discharge curves of Li||NCM811 cells at different temperatures. Reproduced with permission.<sup>[56]</sup> Copyright 2023 Wiley.

### 3. Solvents

#### 3.1. Ether Solvent

Ether-based electrolytes are known for their low melting points and viscosities, which enable them to maintain excellent fluidity even at low-temperature. This characteristic is crucial for sustaining high ionic conductivity under such conditions. Moreover, ether solvents possess a relatively lowest unoccupied molecular orbital (LUMO) level, significantly reducing the reactivity between lithium and nonprotonic organic solvents, thereby enhancing the compatibility of these solvents with the lithium metal anode.

Based on these advantages of ether solvents, researchers have also made significant achievements in ether-based electrolytes. Jin et al. used a low affinity solvent, 1,3-dioxolane (DOL), in

the preparation of electrolyte (LiTFSI-DOL). The rapid desolvation of Li<sup>+</sup> at low-temperature was achieved by adjusting the solvent-solvent interaction environment. Consequently, Li||NCM523 cells still maintain 66% of the room temperature capacity and are able to fast-charge at 0.3 C and -40 °C (Figure 5a).<sup>[57]</sup>

Research on regulating SEI has attracted widespread attention, aiming to address critical issues such as severe side reactions at the electrolyte/electrode interface, deterioration of active materials, and sluggish ion transport. Li et al. developed a tetrahydrofuran (THF)-based localized high-concentration electrolyte containing 1,1,2,2-tetrafluoroethyl-2,2,3,3-tetrafluoropropyl ether (TTE) as a diluent (2 M LiFSI in THF/TTE), which facilitated rapid interfacial defluorination reactions, leading to the formation of an amorphous, inorganic-rich SEI that effectively inhibited the propagation of lithium dendrites (Figure 5b). Consequently, the highly

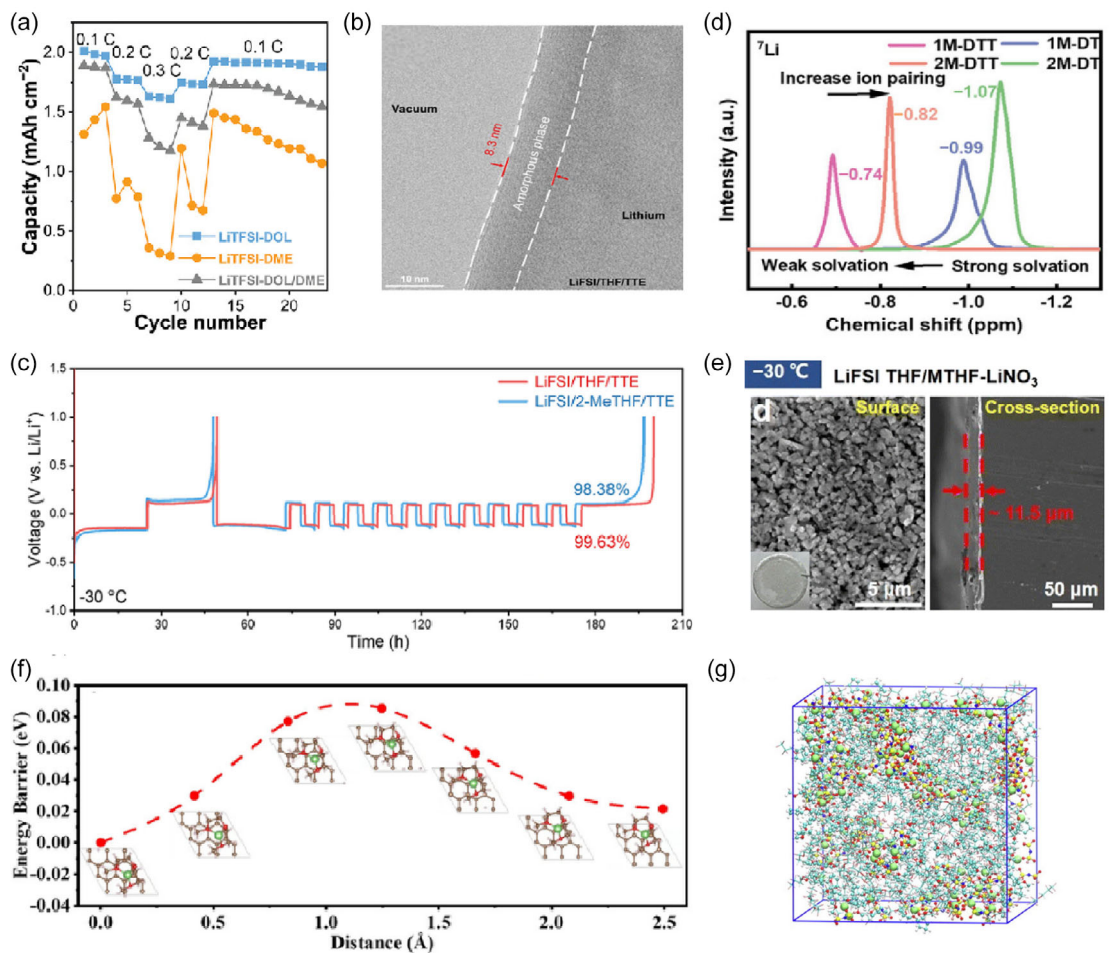


**Figure 5.** a) Rate performance of Li||NCM523 cells at -40 °C. Reproduced with permission.<sup>[57]</sup> Copyright 2022 Wiley. b) High-resolution Cryo-TEM image of SEI formed in the LiTFSI/THF/TTE electrolyte. Reproduced with permission.<sup>[58]</sup> Copyright 2024, American Chemical Society. c) CE curves of Li||Cu cells using Aurbach method in 0.2 mA cm<sup>-2</sup> at -30 °C. Reproduced with permission.<sup>[58]</sup> Copyright 2024 American Chemical Society. d) <sup>7</sup>Li-NMR spectra of different electrolytes. Reproduced with permission.<sup>[59]</sup> Copyright 2024 Wiley. e) SEM image of the top and cross-sectional views of circulating lithium in the LiTFSI THF/MTHF-LiNO<sub>3</sub> electrolyte at -30 °C. Reproduced with permission.<sup>[60]</sup> Copyright 2022 Royal society of chemistry. f) The calculated energy barrier for the diffusion of solvated Li<sup>+</sup> in Gr (the insets illustrate the configurations of the Li-DEGDME complexes at different states during the diffusion process). Reproduced with permission.<sup>[61]</sup> Copyright 2022 Wiley. g) MD simulation snapshots of LiTFSI-2CPME-2TTE electrolytes at 298.15 K. Reproduced with permission.<sup>[62]</sup> Copyright 2024 Elsevier.

reversible lithium metal anode achieved an exceptional CE of up to 99.63% at the low-temperature of -30 °C (Figure 5c).<sup>[58]</sup>

In the process of systematic investigation of ether electrolytes, Gu et al. proposed an innovative strategy. They selected DOL and TTE (2 M LiTFSI in DOL/THF/TTE, 3:3:4 volume ratio). By adjusting the concentration of lithium salts, they successfully increased the proportion of anions in the solvation structure (Figure 5d). This modification led to the formation of a more compact and robust SEI, thereby significantly enhancing the long-term stability and ultra-low-temperature performance of lithium metal batteries. Specifically, Li||Cu cells demonstrated remarkable performance, operating for over 400 h at -40 °C with an average CE of 98.05%. Meanwhile, Li||NCM811 cells also exhibited excellent stability, maintaining 93.7% of their initial capacity after 100 cycles at -40 °C.<sup>[59]</sup>

Yu et al. developed a novel electrolyte system, 1.6 M LiTFSI in THF/2-methyltetrahydrofuran (MTHF) + 2wt% LiNO<sub>3</sub>. The solvent in the electrolyte was characterized by its low reduction potential

and relatively weak solvating ability. Scanning electron microscopy (SEM) analysis of the lithium deposits revealed a dense, dendrite-free morphology with a silver metallic luster when operated at -30 °C (Figure 5e), and the thickness of the deposited lithium reduced from 21.9 to 11.5 μm. Consequently, the Li||LiNi<sub>0.85</sub>Co<sub>0.05</sub>Al<sub>0.1</sub>O<sub>2</sub> cells using this electrolyte was able to maintain a high capacity of 130 mAh g<sup>-1</sup> even after 100 cycles at -30 °C.<sup>[60]</sup>

Later, Yang et al. investigated an electrolyte system combining 1.5 M lithium trifluoride (LiOTF) with 0.2 M LiPF<sub>6</sub> in a mixture of diethylene glycol dimethyl ether (DEGDME) and DOL solvent, achieving coembedding of Li<sup>+</sup> and solvent. Theoretical calculations and experimental characterization revealed that the Li<sup>+</sup>-solvent coembedding process requires no complete stripping of the solvent shell surrounding Li<sup>+</sup>. This cointercalation process exhibited characteristics such as low interfacial resistance, minimal charge transfer activation energy (0.23 eV atom<sup>-1</sup>), and extremely low diffusion barriers (0.09 eV atom<sup>-1</sup>) (Figure 5f), resulting in solvated Li<sup>+</sup> exhibiting diffusion coefficients in Gr that

remain nearly temperature-independent. Consequently, the  $\text{Gr}||\text{NCM811}$  cells demonstrated stable operation at extremely low-temperature, maintaining 73.7% of its room-temperature capacity even at  $-60^\circ\text{C}$ .<sup>[61]</sup>

Zhang et al. designed a diluted high-concentration electrolyte (DHCE) based on cyclopentyl methyl ether (CPME) dilution. Owing to the relatively loose coordination between  $\text{Li}^+$  and CPME, the solvation energy barrier for  $\text{Li}^+$  was significantly reduced. This facilitated the formation of ion clusters, which in turn drove anion-derived interface (Figure 5g). As a result, the compatibility of the lithium metal anode (LMA) was enhanced and the desolvation kinetics of  $\text{Li}^+$  was greatly accelerated, leading to excellent cycling stability. Specifically, the  $\text{Li}||\text{S}$  cells exhibited a capacity retention of up to 70% after 170 cycles at  $-60^\circ\text{C}$ .<sup>[62]</sup>

### 3.2. Ester Solvents

Common ester solvents in electrolyte include carbonate such as EC, DEC and FEC, and carboxylate such as methyl acetate (MA),

EA and ethyl butyrate (EB). Li et al. designed an ester-based electrolyte with methyl propionate (MP) as the main solvent, which has a low freezing point and wide electrochemical stability window. In order to compensate the poor film forming capacity of MP, a small amount of FEC (10 vol%) was added as the cosolvent to enhance the cryogenic ionic conductivity and liquid range of the electrolyte (Figure 6a). As a result, LFP $\parallel$ Gr pouch cells using LiFSI/MF91 (1.5 M LiFSI in MP/FEC) electrolyte can maintain stable cycling performance at  $-20^\circ\text{C}/0.5\text{ C}$  and  $-40^\circ\text{C}/0.1\text{ C}$  (Figure 6b).<sup>[63]</sup>

By introducing fluorine atoms, scientists have changed the electronegativity of ester solvents, thus broadening the liquid range of electrolytes and forming unique solvation structures.<sup>[64]</sup> Chen et al. introduced a novel type of fully fluorinated carboxylate electrolyte, comprising methyl 3,3,3-trifluoropropionate (MTFP) and FEC as the solvents (1 M  $\text{LiPF}_6$  in MTFP/FEC (9:1 v/v)). This electrolyte demonstrated an impressively high ionic conductivity of  $0.75\text{ mS cm}^{-1}$  at  $-60^\circ\text{C}$  (Figure 6c). The incorporation of FEC was found to decrease the  $\text{Li}^+$  solvation energy in comparison to that of EC, allowing the cells using MTFP/FEC-based electrolyte to

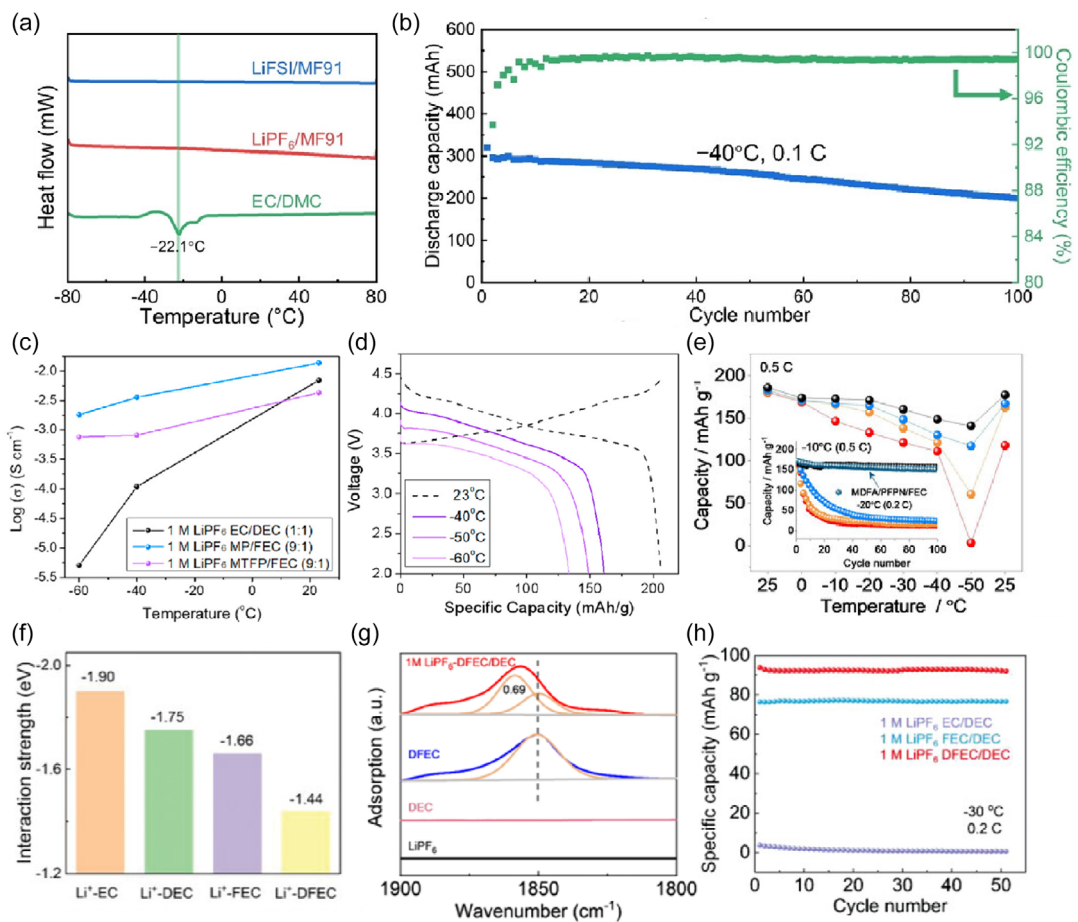


**Figure 6.** a) DSC curves of different electrolytes. Reproduced with permission.<sup>[63]</sup> Copyright 2024, Wiley. b) Cycling performance of the LFP $\parallel$ Gr pouch cells using LiFSI/MF91 at  $-40^\circ\text{C}$  and  $0.1\text{ C}$ . Reproduced with permission.<sup>[63]</sup> Copyright 2024 Wiley. c) Ionic conductivity of selected electrolytes measured at different temperatures. Reproduced with permission.<sup>[65]</sup> Copyright 2020 American Chemical Society. d) Discharge curves of  $\text{Li}||\text{NCM811}$  cells using 1 M  $\text{LiPF}_6$  MTFP/FEC at  $0.1\text{ C}$ . Reproduced with permission.<sup>[65]</sup> Copyright 2020 American Chemical Society. e) Discharge capacity  $\text{Gr}||\text{NCM811}$  cells at different temperatures. (Insert: cycling performance of different electrolytes). Reproduced with permission.<sup>[66]</sup> Copyright 2022 Wiley. f) Deconvoluted ATR-FTIR spectra of carbonyl groups (EC, FEC, DFEC) in 1 M  $\text{LiPF}_6$ -DFEC/DEC electrolytes. Reproduced with permission.<sup>[67]</sup> Copyright 2021 Wiley. g) The interaction strength between  $\text{Li}^+$  and polar solvents obtained by first-principles calculations. Reproduced with permission.<sup>[67]</sup> Copyright 2021 Wiley. h) Cycling performances of NCM811 $\parallel$ Li cells at  $-30^\circ\text{C}$ . Reproduced with permission.<sup>[67]</sup> Copyright 2021 Wiley.

maintain 66.2% of the room temperature capacity even at the low-temperature of  $-60^{\circ}\text{C}$  (Figure 6d).<sup>[65]</sup> Zou et al. meticulously engineered the methyl difluoroacetate (MDFA)/FEC-based electrolyte ( $\text{LiPF}_6$ :MDFA: PFPN: FEC (1:7:0.5:1 molar ratio)), leveraging fluorinated carboxylate as the foundational components. Owing to its remarkably low freezing point, the Gr||NCM811 cells using this electrolyte can deliver a discharge capacity retention of 75.8% of its room-temperature capacity at an extremely low-temperature of  $-50^{\circ}\text{C}$ , under a current density of 0.5 C (Figure 6e).<sup>[66]</sup> In addition, Wang et al. conducted a comparative analysis of EC, FEC, and difluoroethylene carbonate (DFEC) solvents. They observed that as the degree of fluorination increased, the ion-dipole interaction strength between  $\text{Li}^+$  and the polar solvent dipoles progressively decreased, from 1.90 eV for EC to 1.66 eV for FEC, and further to 1.44 eV for DFEC (Figure 6f). Concurrently, the coordination ratio of  $\text{Li}^+$  also diminished, from 0.84 in EC to 0.76 in FEC, and finally to 0.69 in DFEC (Figure 6g). Even in a DFEC/DEC-based electrolyte at  $-30^{\circ}\text{C}$ , the Li||NCM811 cells can still achieve 51% of its room-temperature capacity (Figure 6h),<sup>[67]</sup> highlighting the significant impact of fluorination on the electrolyte's low-temperature performance.

Liu et al. utilized iso-butyl formate (IF) as an antifreezing agent, dissolving 1 mol L<sup>-1</sup> LiODFB in FEC/DMS/IF to achieve low coordination number, high de-solvatization energy, and high  $\text{Li}^+$  saturation concentration, enabling efficient and reversible lithium-ion transfer. NMR results revealed the presence of significant LiF components. During the charge-discharge process, a substantial amount of LiF forms induced by the electrolyte containing 45% IF. This led to the formation of stable LiF-rich SEI (10.48 wt%) and CEI (17.91 wt%). As a result, Li||LCO cells using this electrolyte can deliver over 170 cycles of stable capacity at  $-70^{\circ}\text{C}$ , with discharge capacity remaining at 110 mAh g<sup>-1</sup>.<sup>[68]</sup>

Wang et al. have introduced a groundbreaking asymmetric solvent-regulated crystallization limitation strategy: they selected ethylene sulfite (ES), which features weaker, compared with C=O, polar S=O groups and asymmetric structure, as main solvent, and FEC that possesses high electronegativity as cosolvent. During the freezing process, this innovative solvent system exhibits only minor enthalpic changes. This subtle alteration effectively reduces the molecular interactions and orientation dynamics within the electrolyte. As a result, the electrolyte is capable of sustaining rapid ion transport even at extremely low-temperature of  $-50^{\circ}\text{C}$ , thereby enabling the NCM811||Li cells to deliver excellent temperature resilience and cycling stability over a wide temperature range from  $-50$  to  $70^{\circ}\text{C}$ .<sup>[69]</sup>

Guided by density functional theory (DFT) calculation, Xu et al. proposed an innovative strategy for solvent screening, targeting those with low donor numbers (DN, less than 10) and moderate dielectric constants (greater than 5), which is adopted to identify solvents that exhibit weak binding energy with  $\text{Li}^+$  while still possessing the capability to fully dissociate lithium salts. By minimizing the  $\text{Li}^+$ -solvent binding energy during low-temperature and fast-charging processes, these solvents can effectively dissociate lithium salts without compromising performance. They used MDFA and methyl 2,2-difluoro-2-(fluorosulfonyl)acetate (MDFSA) as solvents. As a result, Gr||NMC811 full

cells achieved a remarkable capacity retention of 93.9% after 260 cycles at  $-30^{\circ}\text{C}$  with an average CE of 99.98%.<sup>[70]</sup>

### 3.3. Nitrile Solvents

Nitrile solvents also play a significant role in the low-temperature electrolytes. These solvents have low freezing points, which significantly enhance the fluidity of the electrolyte at low-temperature. Additionally, they have high dielectric constants, which facilitate the dissociation of lithium salts, leading to more freely mobile ions and thus increasing ionic conductivity.

Lu et al. proposed a novel approach to design cryogenic electrolytes by utilizing small-size solvents with low solvent energy. Through careful screening, they identified fluoroacetonitrile (FAN) as an optimal solvent due to its low  $\text{Li}^+$  transport energy barrier, low solvation energy, and small solvation shell volume. Within the electrolyte, FAN forms a dual-solvation structure: the small solvent molecules in the secondary solvation sheath interact with the internal  $\text{Li}^+$ , while the primary solvation sheath releases  $\text{Li}^+$ , creating a fast ion-conducting ligand channel that enhances  $\text{Li}^+$  transport. Additionally, the weak solvation ability of FAN allows anions to enter the primary solvation shell, thereby forming an inorganic-rich interfacial layer. As a result, Gr||NMC811 full cells achieved remarkable performance at ultra-low-temperature: at  $-35$ ,  $-60$ , and  $-80^{\circ}\text{C}$ , the cells maintained capacities of 76% (164.8 mAh g<sup>-1</sup>), 63% (135.0 mAh g<sup>-1</sup>), and 51% (109.7 mAh g<sup>-1</sup>), respectively.<sup>[71]</sup>

Luo et al. used DFT to calculate the electron density ( $\rho(r)$ ) and potential energy density ( $V(r)$ ) at the critical point of the bond (BCP) to determine the interaction strength. They identified isobutyronitrile (iBN) as the cosolvent with the lowest  $\rho(r)$  and  $V(r)$ , thereby indicating its weakest interaction with  $\text{Li}^+$ . Due to the poor reduction stability of iBN, EC was added to the electrolyte to prevent its reduction and decomposition. It was discovered that when the iBN content was increased to 60%, the viscosity of the electrolyte was significantly reduced while dissociation degree of the lithium salt was highly enhanced. Consequently, the electrolyte maintained a conductivity of up to 1.152 mS cm<sup>-1</sup> at  $-70^{\circ}\text{C}$ , enabling the Gr||LCO pouch cells to deliver 68.7% of its room-temperature capacity at  $-70^{\circ}\text{C}$ .<sup>[72]</sup>

### 3.4. Other Solvents

In addition to the above traditional solvent modification strategies, scientists have also explored a variety of new strategies, such as new amphiphilic solvents, cosolvents, organic silicon electrolytes, high-entropy solvents, and diluents.

Shi et al. have developed a novel amphiphilic solvent, 1,1,2,2-tetrafluoro-3-methoxypropane (TFMP), which features a molecular structure incorporating both lithiophilic ( $-\text{O}-$ ) and lithiophobic ( $-\text{CF}_2\text{CF}_2\text{H}$ ) components. This unique molecular structure promotes the self-assembly of the electrolyte into a distinctive core-shell solvation structure (Figure 7a). The solvent exhibits weak  $\text{Li}^+$ -solvent interactions and a low coordination number in the solvation sheath, thereby achieving a relatively high ionic conductivity and suppressed solvent cointercalation. These properties

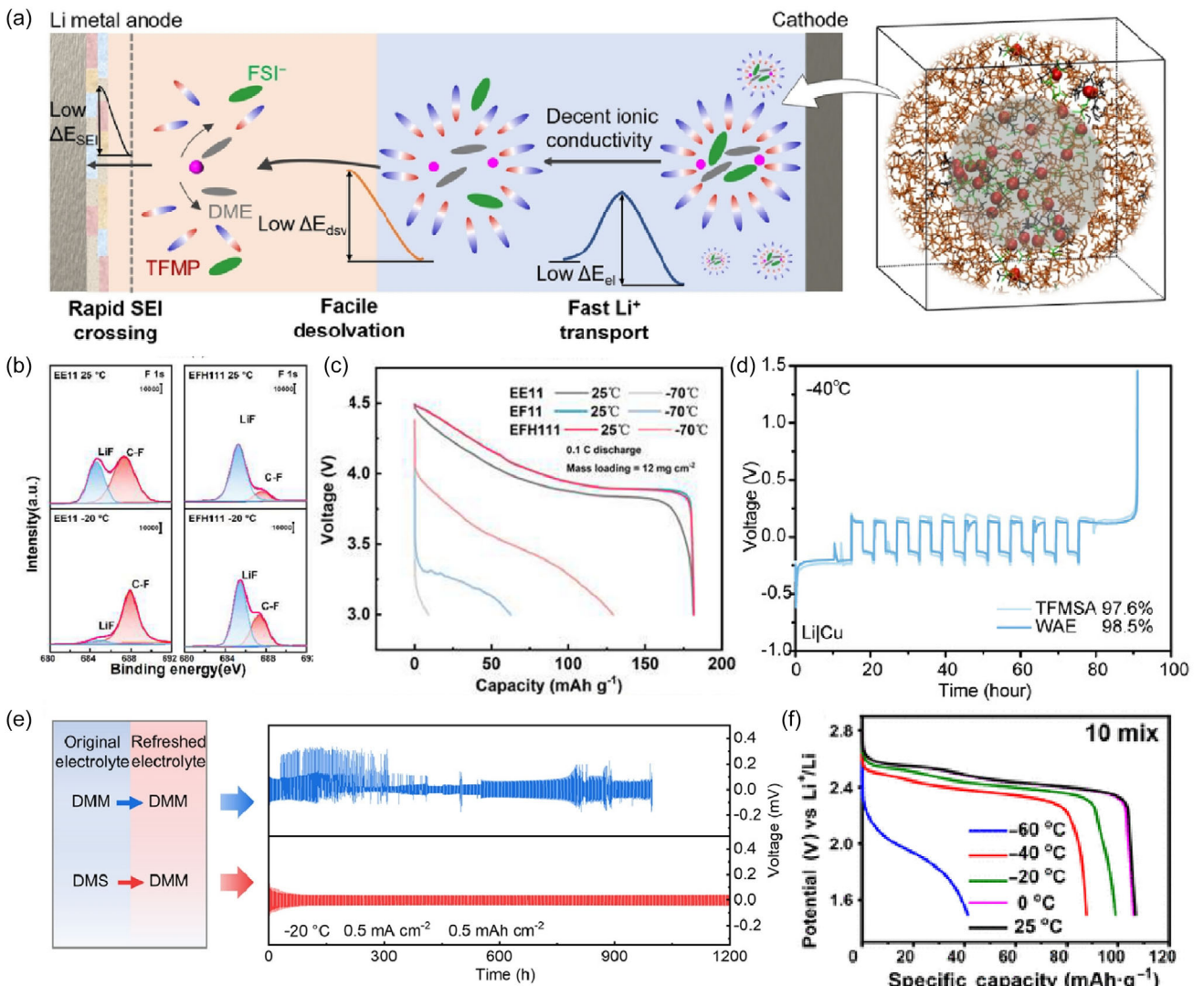


**Figure 7.** a) Schematic illustration of fast electrochemical kinetics induced by the core-shell-solvation structure in 1 M LiFSI-TFMSA/DME electrolyte considering all the three steps that affect Li<sup>+</sup> transport during charging. Reproduced with permission.<sup>[73]</sup> Copyright 2023, Wiley. b) F1s XPS profiles of the cycled Li metal anode at room and -20 °C. Reproduced with permission.<sup>[74]</sup> Copyright 2024 Elsevier. c) Voltage profile during discharge of high loading cathode Li||LCO cells in electrolytes at 25 and -70 °C. Reproduced with permission.<sup>[74]</sup> Copyright 2024 Elsevier. d) Voltage profiles of Li||Cu half cells at -40 °C at a current density of 0.33 mA cm<sup>-2</sup>.<sup>[75]</sup> Copyright 2023 Wiley. e) Solvent exchange experiments on Li||Li cells. Reproduced with permission.<sup>[76]</sup> Copyright 2025 Cell Press. f) Discharging curves of LMO||LTO full cell with decimal solvent-based electrolytes at 0.1 C at various temperatures. Reproduced with permission.<sup>[77]</sup> Copyright 2021 Chinese Chemical Society.

contribute to the formation of a highly robust and conductive SEI, effectively overcoming the long-standing challenges of lithium compatibility and deposition dynamics. Consequently, this innovation enables lithium metal batteries to operate efficiently at ultra-low-temperature: Li||NMC811 cells can charge and discharge at 0.5 C and exhibit stable cycling for over 100 cycles at 0.2 C, even at -40 °C.<sup>[73]</sup>

Lai et al. designed an electrolyte of 1 M LiPF<sub>6</sub> in the ethyl methyl carbonate (EMC)/FEC/1,1,2,2-tetrafluoroethyl-2,2,2-trifluoroethyl ether (HFE), named EFH111. The addition of partially fluorinated solvent not only weakens the solvation ability due to the strong electronegativity of the F atoms on the fluorinated solvent but also improves the temperature adaptability of the solvation structure due to its structural asymmetry. Even at

low-temperature, uniform lithium deposition, faster charge transfer kinetics or SEI kinetics, and inorganic-rich components in the SEI can be achieved (Figure 7b). Therefore, the EFH111 electrolyte can maintain 71.4% of the room-temperature discharge capacity at -70 °C (Figure 7c).<sup>[74]</sup> Wang et al. introduced a rational design strategy for wide-temperature electrolytes by carefully selecting weak solvents and antisolvents, in which weak solvent, N,N-dimethyltrifluoromethane-sulfonamide (TFMSA), significantly enhances the desolvation kinetics of Li<sup>+</sup> near the anode region, thereby improving the electrochemical performance. Meanwhile, the antisolvent, TTE, plays a dual role: It acts as a cryogenic agent to facilitate ion migration at low-temperature and interacts synergistically with the weak solvent TFMSA to promote ion aggregation. The combination of TFMSA and TTE ensures

both high ionic conductivity and thermal stability. The resulting weak antisolvent electrolyte (0.75 M LiFSI-TFMSA/TTE (7:3 v/v)) demonstrates excellent compatibility with both lithium metal and Gr electrodes. At  $-40^{\circ}\text{C}$ , the lithium anode achieves a remarkable CE of 98.5%, and the Gr electrode exhibits a discharge capacity exceeding  $230 \text{ mAh g}^{-1}$  (Figure 7d). Furthermore, a  $4.2 \text{ mAh cm}^{-2}$  Li||LCO cells utilizing this weak antisolvent electrolyte can deliver a capacity of 73.8% at  $-40^{\circ}\text{C}$ .<sup>[75]</sup>

Yin et al. successfully developed an organic SEI that is rich in Si—O bonds using organic silicon electrolytes: 1.5 M LiFSI in dimethyl dimethoxy silane. Compared with traditional organic SEI (e.g., those containing  $\text{ROCO}_2\text{Li}$ , ROLi, etc.), this Si—O-rich SEI demonstrates significantly suppressed decomposition and reconstruction during long-term cycling, thereby maintaining excellent mechanical properties and chemical stability (Figure 7e). Additionally, it substantially lowers interfacial impedance and overpotential, resulting in a remarkable enhancement in the charging and discharging performance of cells under low-temperature. For instance, the capacity retention of Li||NCM811 cells after 180 cycles at  $-40^{\circ}\text{C}$  reached an impressive 95.2%.<sup>[76]</sup>

In addition to increasing the entropy value through the addition of lithium salts, expanding the variety of solvents can also enhance the degree of disorder. As a proof of concept, Zhang et al. designed a high-entropy electrolyte using a decimal solvent. This molecularly disordered solvent mixture effectively suppresses the freezing crystallization of the electrolyte, thereby reducing its freezing point to as low as  $-130^{\circ}\text{C}$ . Moreover, it maintains a high conductivity of  $0.62 \text{ mS cm}^{-1}$  even at  $-60^{\circ}\text{C}$ . As a result,  $\text{LiMn}_2\text{O}_4$  (LMO) ||  $\text{Li}_4\text{Ti}_5\text{O}_{12}$  (LTO) cells utilizing this electrolyte can retain 80% of their room-temperature capacity at  $-40^{\circ}\text{C}$  (Figure 7f).<sup>[77]</sup>

Nan et al. recently proposed a novel electrolyte known as low-polarity-solvent electrolytes (LPSEs), which incorporates a diluent, 1,1,2,2-tetrafluoro-3-(1,1,2,2-tetrafluoroethoxy) propane (TFTP). Compared to other highly polar solvents, TFTP exhibits significantly weaker ion-dipole interactions, thus effectively reducing the electrical resistance and activation energy associated with the charge-transfer process, thereby enhancing the kinetic during the desolvation step (Figure 8a). Additionally, LPSEs possess an intrinsic ability to form partially dissociated salt domains, characterized by a high proportion of CIPs and AGGs, resulting into anion-derived, inorganic-rich, and stable EEIs with excellent  $\text{Li}^+$  transport properties. Gr||NCM811 cells using this electrolyte demonstrated remarkable cycling stability and high capacity retentions, achieving 84% and 78% at  $-30$ ,  $-40^{\circ}\text{C}$ , respectively.<sup>[78]</sup>

Liu et al. developed a LHCE by incorporating a diluent, TTE (7 M LiFSI: AN: TTE (1: 2.73: 5.66 molar ratio)). In LHCE, the elevated lithium salt concentration promoted more anions to participate in the solvation structure of  $\text{Li}^+$ , thus forming an inorganic-rich CEI/SEI, which significantly reduce interfacial impedance and improves  $\text{Li}^+$  transport efficiency. Moreover, the coordinated effect of the diluent mitigates the high viscosity typically associated with concentrated electrolytes, while preserving its unique solvation structure. This dual-action mechanism notably enhances ionic conductivity and interfacial stability, especially at

low-temperature. As a result, Li||NMC811 cells achieve a capacity retention up to 85.5% after 95 cycles at  $-30^{\circ}\text{C}$  (Figure 8b).<sup>[79]</sup>

John et al. innovatively introduced bis(2,2,2-trifluoroethyl) ether (BTFE) as a diluent into the LiFSI-DEE electrolyte system (LiFSI in DEE/BTFE (1:2.6:2 mol ratio)). Their findings revealed that the incorporation of BTFE effectively weakened the binding interactions between the solvents and  $\text{Li}^+$ , thus simultaneously optimizing the local solvation structural environment, both of which significantly enhanced the charge transfer kinetics associated with solvent removal during the electrochemical process. The local dilution by BTFE promoted a more universal distribution of structural states with minimal nonzero coordination solvents. It also reduced the size of long-range ion AGGs, facilitating a simpler and more efficient removal of lithium solvation shells (Figure 8c). As a result, the cells using this electrolyte exhibited remarkable electrochemical reversibility, even at extremely low-temperature down to  $-60^{\circ}\text{C}$ . Moreover, the electrolyte endows rapid charging capabilities, with a charging time as short as 20 min. This work highlights the potential of BTFE as an effective dilute for improving the low-temperature performance and fast-charging characteristics of lithium-based batteries.<sup>[80]</sup>

## 4. Additives

Although the additive accounts for only 0.1–10 wt% of the total electrolyte, it can precisely modulate the  $\text{Li}^+$  solvation sheath at the molecular level and reconstruct the electrolyte-electrode interphases, thereby simultaneously reducing the interfacial impedance and expanding the operating temperature windows of lithium-based batteries.<sup>[81]</sup> To systematically elucidate the structural linkages, we classify the reported additives into two functional categories: film formation additives and solvation structure modulating additives.

For the film formation additives, Thenuwara et al. introduced a small amount of FEC carbonate additive into the DOL/DME electrolyte, which significantly improved the low-temperature cycling stability of Li||LFP cells at  $-40^{\circ}\text{C}$  (0.8 M LiTFSI + 0.2 M LiNO<sub>3</sub> in DOL/DME + 10 vol% FEC). The CE remained above 98% after 12 cycles (Figure 8d). This was attributed to the strong coordination between FEC and  $\text{Li}^+$  at low-temperature, enabling it to preferentially enter the first solvation shell, displacing part of DOL and altering the reduction sequence. This induced the formation of an inorganic SEI rich in LiF and  $\text{Li}_2\text{CO}_3$ .<sup>[82]</sup> Lithium salt additives are another common type of additives that promote the formation of interfacial films. By incorporating a small amount of LiBF<sub>4</sub> into the DMC/EMC cosolvent (0.7 M LiPF<sub>6</sub> + 0.3 M LiBF<sub>4</sub> in DMC/EMC (3/5 w/w) + 16 vol% BA + 10 vol% EC), Lv et al. observed that after 50 cycles at  $-40^{\circ}\text{C}$ , the cathode electrode exhibited a denser and more uniform CEI with a thickness of merely 22.4 nm (Figure 8e). This enhanced protection for the cathode material significantly improved low-temperature performance. Consequently, the Li||NCM811 cells maintained a capacity of  $75 \text{ mAh g}^{-1}$  even after 50 cycles at  $-40^{\circ}\text{C}$ .<sup>[83]</sup>

Another strategy to improve temperature adaptability is to add functional additives to improve the solvation structure of

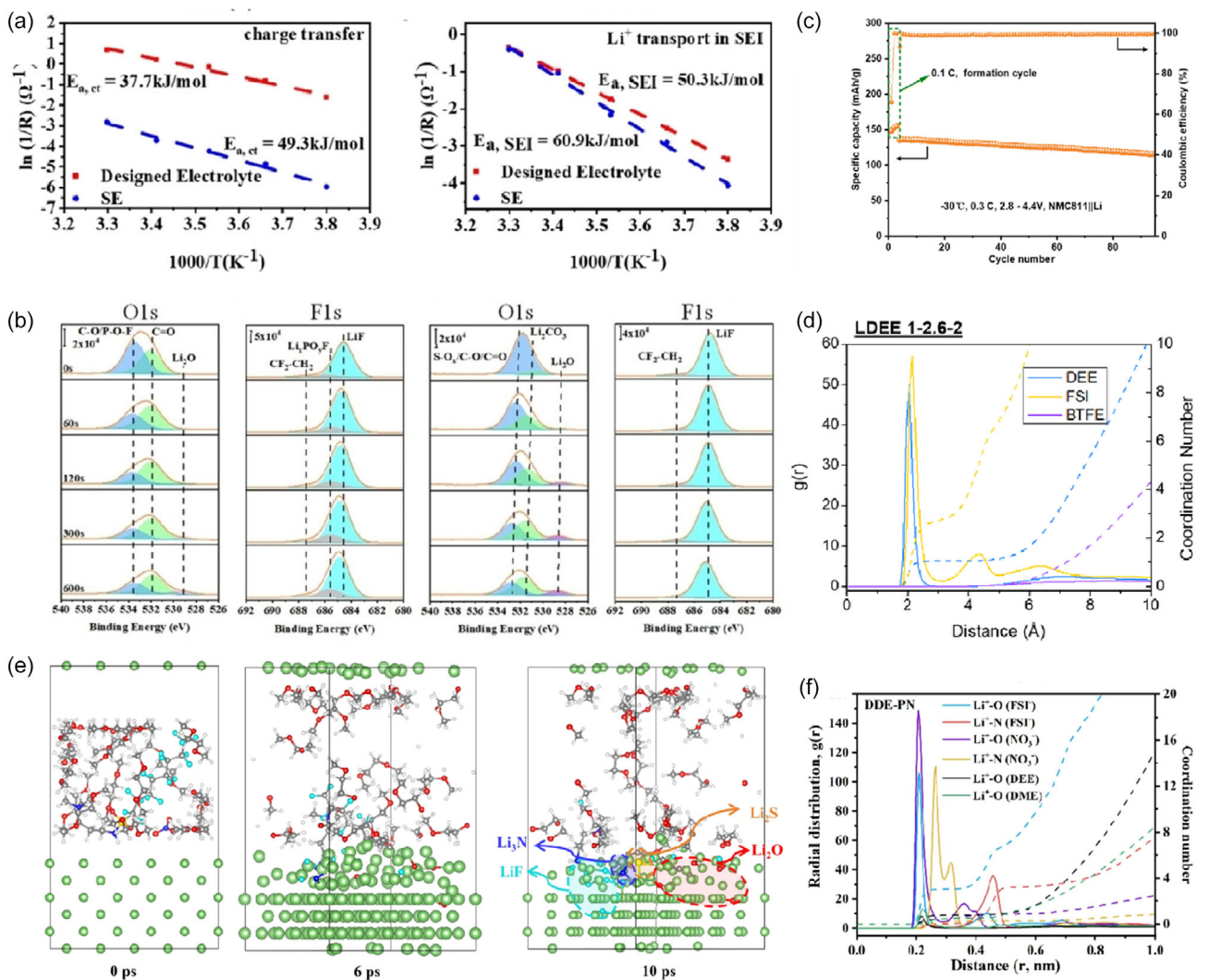


**Figure 8.** Activation energies of a) the charge transfer process and Li<sup>+</sup> transport in the SEI of the Gr with designed electrolyte and standard electrolyte. Reproduced with permission.<sup>[78]</sup> Copyright 2022, Wiley. b) Cycling performances of Li||NMC811 cells at low-temperature. Reproduced with permission.<sup>[79]</sup> Copyright 2024 Royal society of chemistry. c) Radial distribution functions of various solvating components with respect to Li<sup>+</sup>. Reproduced with permission.<sup>[80]</sup> Copyright 2023 PNAS. d) Charge and discharge profiles of Li||LFP cell at -40 °C (inset is the CE data for 12 charge and discharge cycles at -40 °C). Reproduced with permission.<sup>[82]</sup> Copyright 2020 American Chemical Society. e) TEM image of Li||NMC811 cell after 50 cycles at -40 °C. Reproduced with permission.<sup>[83]</sup> Copyright 2021 Elsevier. f) Radial distribution functions and coordination numbers in DDE-PN. Reproduced with permission.<sup>[84]</sup> Copyright 2025 Nature Publishing Group.

lithium. Zhang et al. have ingeniously designed and synthesized a multifunctional additive known as perfluoroalkylsulfonyl quaternary ammonium nitrate (PQA-NO<sub>3</sub>), which is composed of cations (PQA<sup>+</sup>) and anions (NO<sub>3</sub><sup>-</sup>). The cation PQA<sup>+</sup> can react with lithium metal to form a SEI that is rich in inorganic components, which enhances the transport capability of Li<sup>+</sup> through the interphases, thereby improving the overall kinetics. Meanwhile, the anion NO<sub>3</sub><sup>-</sup> constructs a solvation structure that is rich in anions but depleted in solvent molecules (Figure 8f). This unique solvation structure not only improves the oxidation stability at the cathode/electrolyte interface but also reduces the interactions between Li<sup>+</sup> and solvents. Consequently, Li||NMC811 pouch cells demonstrates remarkable stable cycling performance even at extremely low-temperature of -60 °C.<sup>[84]</sup>

Besides the above discussion, we have summarized the representative low-temperature electrolytes and the corresponding electrochemical performances in this review, as shown in Table 1. First, the introduction of low melting point/low viscosity cosolvent (EA, DEGDME, IF, etc.) or high entropy can reduce the freezing point of the electrolyte, improve the ionic conductivity, and broaden the working temperature of the electrolyte. Secondly, the Li<sup>+</sup> first solvation shell is transferred from over-coordinated SSIP to CIP/AGG configuration in the weakly solvating electrolyte, highly concentrated electrolytes, or localized highly concentrated electrolytes, in which the desolvation energy barrier and/or the charge transfer impedance at low temperatures were reduced by orders of magnitude. Finally, LiNO<sub>3</sub>, LiPO<sub>2</sub>F<sub>2</sub>, FEC, or siloxanes are used to construct electrode-electrolyte interphases rich in

**Table 1.** Typical electrolytes and their effects on electrochemical performance of lithium-based batteries.

Electrolyte	Cell configuration	Test condition (temperature, voltage, and rate)	Capacity retention/ cycles	CE	Reference
<b>Lithium salts</b>					
1.5 M LiTFSI-BFPE	Li  NCM811	–40 °C, 2.5–4.3 V 0.1 C charge/discharge	>92%, 100	98.8% (-30 °C)	[49]
1 M LiPF <sub>6</sub> in DMC/EMC (3:5 w/w) + 4 vol% PC + 0.2 vol% FEC + 2 wt%LiPO <sub>2</sub> F <sub>2</sub>	Li  NCM811	–40 °C, 2.8–4.2 V 0.2 C charge/discharge	81.94 mAh g <sup>-1</sup> , 50	99.8% (-20 °C)	[50]
0.6 M LiFSI + 0.4 M LiDFOB in DMS	Gr  LCO pouch cells	–50 °C, 2.5–4.3 V 0.1 C charge/discharge	86%, 250	–	[51]
LiFSI + LiODFB (7:3 molar ratio) in MA/FEC (8:2 v/v) + 0.15 M kg <sup>-1</sup> LiNO <sub>3</sub>	Li  NCM523	–40 °C, 2.8–4.3 V 0.2 C charge/discharge	84%, 150	–	[52]
0.1 M LiFSI + 0.9 M LiODFB in EA/FEC (95:5 v/v)	2.5 Ah LFP  Gr Pouch cell	–40 °C, 2.0–4.0 V 0.1 C charge/discharge	66.28%, 1	–	[53]
0.6 M LiFSI + 0.2 M LiNO <sub>3</sub> + 0.2 M LiPO <sub>2</sub> F <sub>2</sub> in G2	Li  NCM811	–30 °C, 2.9–4.4 V 0.1 C charge/discharge	88.4%, 200	98.3% (-30 °C)	[54]
0.5 M LiDFOB + 0.2 M LiPO <sub>2</sub> F <sub>2</sub> + 0.3 M LiPF <sub>6</sub> in EC/DEC (1:1 v/v)	Li  NCM811	–30 °C, 2.7–4.7 V 0.2 C charge/discharge	92 mAh g <sup>-1</sup> , 200	–	[55]
0.15 M LiPF <sub>6</sub> /0.15 M LiFSI/0.15 M LiTFSI/0.15 M LiDFOB/0.15 M LiNO <sub>3</sub> in PC/DEC (1:1 w/w) + 5% FEC	Li  NCM811	–50 °C, 2.5–4.3 V 0.1 C discharge	≈110 mAh g <sup>-1</sup> , 1	>80% (-40 °C)	[56]
<b>Solvents</b>					
LiTFSI-DOL	Li  NCM523	–40 °C, 3.0–4.3 V 0.1 C charge/discharge	66%, 1	–	[57]
2 M LiFSI in THF/TTE	Li  LFP	–40 °C, 2.6–3.8 V 0.1 C charge/discharge	70 mAh g <sup>-1</sup> , 1	99.63% (-30 °C)	[58]
2 M LiTFSI in DOL/THF/TTE (3:3:4 v/v)	Li  NCM811	–40 °C, 2.8–4.3 V 0.1 C charge/discharge	93.6%, 100	99.05% (-40 °C)	[59]
1.6 M LiFSI in THF/MTHF + 2wt% LiNO <sub>3</sub>	Li   LiNi <sub>0.85</sub> Co <sub>0.05</sub> Al <sub>0.1</sub> O <sub>2</sub>	–30 °C, 2.8–4.1 V, 0.1 C charge/discharge	130 mAh g <sup>-1</sup> , 100	–	[60]
1.5 M LiOTF + 0.2 M LiPF <sub>6</sub> in DEGDME/DOL (1:1)	Gr   LiNi <sub>0.65</sub> Co <sub>0.15</sub> Mn <sub>0.2</sub> O <sub>2</sub>	–40 °C, 4 V 0.1 C charge/0.3 C discharge	84.5%, 100	–	[61]
LiFSI in CPME/TTE (1:2:2 mol ratio)	Li  S Pouch cell	–60 °C, 1.0–3.0 V 0.05 C charge/discharge	70%, 170	95% (-60 °C)	[62]
1.5 M LiFSI in MP/FEC(9:1 v/v)	Li  LFP	–30 °C, 2.0–4.2 V 0.1 C charge/discharge	88%, 100	–	[63]
1 M LiPF <sub>6</sub> in MTFP/FEC (9:1 v/v)	Li  NCM811	–60 °C, 2.8–4.5 V 0.1 C discharge	133 mAh g <sup>-1</sup> , 1	–	[65]
LiPF <sub>6</sub> : MDFA: PFPN: FEC (1:7:0.5:1)	Gr  NMC811	–50 °C, 2.8–4.3 V 0.5 C discharge	75.8%, 1	–	[66]
1 M LiPF <sub>6</sub> in DFEC/DEC	Li  NCM811	–30 °C, 2.7–4.5 V 0.2 C charge/discharge	≈90 mAh g <sup>-1</sup> , 50	–	[67]
1 M LiDFOB-FEC/DMS/IF	Li  LCO	–70 °C, 2.7–4.5 V 1/15 C charge/discharge	110 mAh g <sup>-1</sup> , 170	–	[68]
1 M LiClO <sub>4</sub> in ES/10%FEC	Li  NCM811	–50 °C, 2.7–4.3 V 0.05 C discharge	139.8 mAh g <sup>-1</sup> , 1	93.33% (-50 °C)	[69]
1 M LiTFSI MDFA/MDFSA-TTE	Gr  NCM811	–30 °C, 2.5–4.5 V 0.2 C charge/discharge	93.9%, 260	–	[70]
1.3 M LiFSI in FAN	Gr  NMC811	–60 °C, 2.8–4.5 V charge/discharge	80%, 350	–	[71]

**Table 1.** Continued.

Electrolyte	Cell configuration	Test condition (temperature, voltage, and rate)	Capacity retention/ cycles	CE	Reference
1 M LiPF <sub>6</sub> in 8.33 vol% EC/31.67 vol% EMC/60 vol% iBN	LCO  Gr Pouch cell	–70 °C, 3–4.1 V 0.1 C discharge	68.7%, 1	–	[72]
1 M LiFSI in TFMP/DME (7:1 v/v)	Li  NCM811	–40 °C, 2.8–4.3 V 0.2 C charge/discharge	≈85 mAh g <sup>−1</sup> , 100	98.5% (–40 °C)	[73]
1 M LiPF <sub>6</sub> in EMC/FEC/HFE(1:1:1)	Li  LCO	–40 °C, 3.0–4.5 V 0.2 C charge/0.5 C discharge	73.6%, 250	97.0% (–20 °C)	[74]
0.75 M LiFSI -TFMSA/TTE(7:3 v/v)	Gr  LCO	–40 °C, 2.5–4.3 V 0.1 C discharge	73.8%, 1	98.5% (–40 °C)	[75]
1.5 M LiFSI in DMS	Li  NCM811	–40 °C, 2.8–4.7 V 0.1 C charge/discharge	95.2%, 180	94.52% (–40 °C)	[76]
1 M LiPF <sub>6</sub> in EC/DEC/PC/EMC/EP/EA/MB/BA/MP/PB	LMO  LTO	–40 °C, – 0.2 C charge/discharge	≈70 mAh g <sup>−1</sup> , 40	–	[77]
LiFSI in EMC/TTE (2:3.3:3.3 mol ratio)	Gr  NCM811	–40 °C, 2.5–4.4 V 0.1 C discharge	54.5%, 1	–	[78]
7 M LiFSI:AN:TTE (1:2.73:5.66 mol ratio)	Li  NMC811	–30 °C, 2.8–4.4 V 0.3 C charge/discharge	85.5%, 95	–	[79]
LiFSI in DEE/BTFE (1:2.6:2 mol ratio)	Li   LiNi <sub>0.8</sub> Co <sub>0.15</sub> Al <sub>0.05</sub> O <sub>2</sub>	–60 °C, 2.0–4.5 V 0.1 C charge/0.2 C discharge	93%, 100	98.9% (–60 °C)	[80]
<b>Additives</b>					
0.8 M LiTFSI + 0.2 M LiNO <sub>3</sub> in DOL/DME + 10 vol% FEC	Li  LiFePO <sub>4</sub>	–40 °C, 2.5–4.0 V 0.05 C charge/discharge	≈76 mAh g <sup>−1</sup> , 10	98% (–40 °C)	[82]
0.7 M LiPF <sub>6</sub> + 0.3 M LiBF <sub>4</sub> in DMC/EMC (3/5 w/w) + 16 vol% BA + 10 vol% EC	Li  NMC811	–40 °C, 2.75–4.2 V 0.2 C charge/discharge	≈75 mAh g <sup>−1</sup> , 50	–	[83]
1 M LiFSI in DME/DDE(9:1 v/v) + 0.1 M PQA-NO <sub>3</sub>	Li  NMC811	–60 °C, 2.8–4.3 V 0.05 C charge/0.1 C discharge	93.3%, 100	97.5% (–60 °C)	[84]

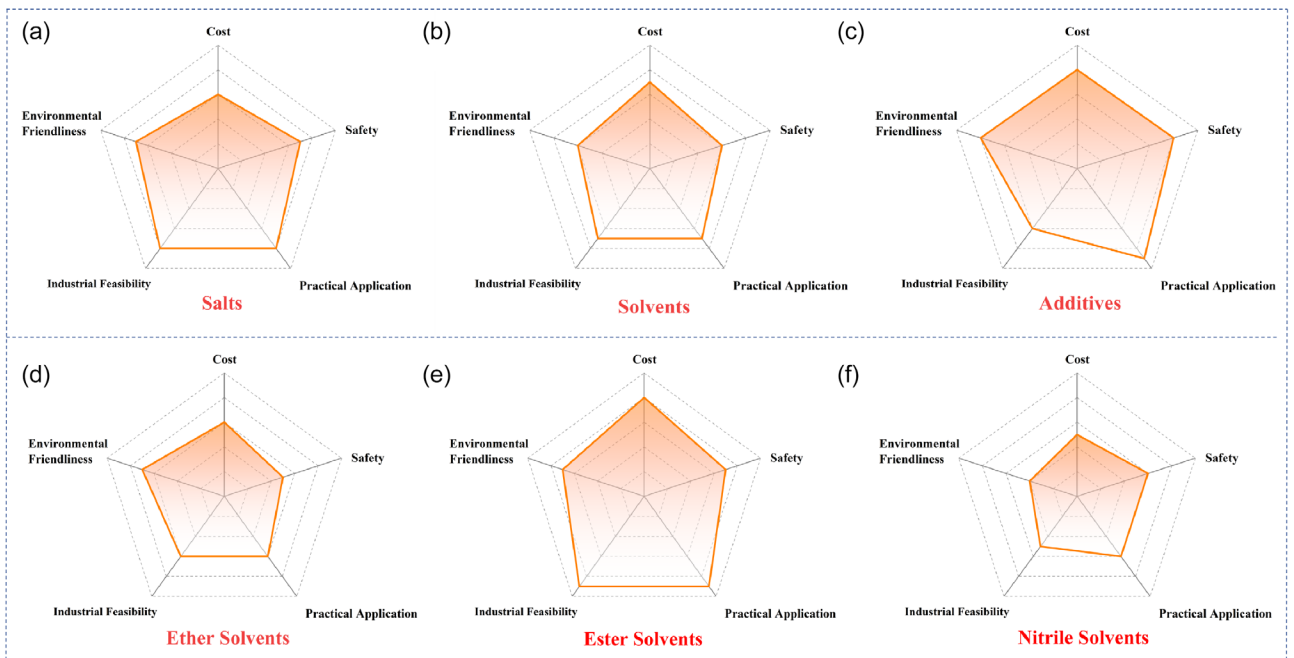


**Figure 9.** Radia plots of a) salts, b) solvents, c) additives, d) ether solvents, e) ester solvents, and f) nitrile solvents' regulation strategies in various aspects.

inorganic components such as LiF or Si—O bonds, which inhibit lithium dendrites and stabilize electrode-electrolyte interphases and thus improve the cycle stability of LIBs.

At present, the widely used lithium salt in commercial LIBs is LiPF<sub>6</sub>, lithium salts used in low temperature LIBs, such as LiFSI and LiTFSI, are usually very expensive and corrosive. For solvents, ester solvents are dominate solvents in the commercial electrolytes due to their excellent overall performance in daily life, low cost, and high safety. But their application at low temperatures is severely inhibited due to their high melting points (such as EC), high viscosity, or high desolvation energy. Ether solvents show high potential in low-temperature electrolytes due to their low melting points and low viscosity, but they usually exhibit inferior oxidation stability, especially in LIBs with high-voltage cathodes. Meanwhile, the fluorinated ethers are confronted with high cost and environmental issues. Other solvents, such as nitrile, used at low temperatures, do not show obvious advantages in cost, environmental friendliness, safety, industrial feasibility. Moreover, they also show poor compatibility with anodes (graphite or

lithium metal) or cathodes. Though additives play key roles in alleviating cycling stability or temperature adaptability, one or two additives cannot meet the requirements of LIBs with excellent cycling stability, high safety, superior temperature adaptability, and enhanced kinetics, which are usually the results of the synergy of multiple additives and/or solvents. Besides, due to the small proportion of additives in the electrolytes, they usually have issues about high cost and industrial feasibility (Figure 9). Making up for the shortcomings of various regulatory strategies is crucial to promote the development of cryogenic electrolytes and further address the many shortcomings faced by current battery technology.

## 5. Conclusion

In summary, this article provides a comprehensive overview and in-depth analysis of various methods for designing electrolyte compositions, aimed at inhibiting lithium dendrite growth,

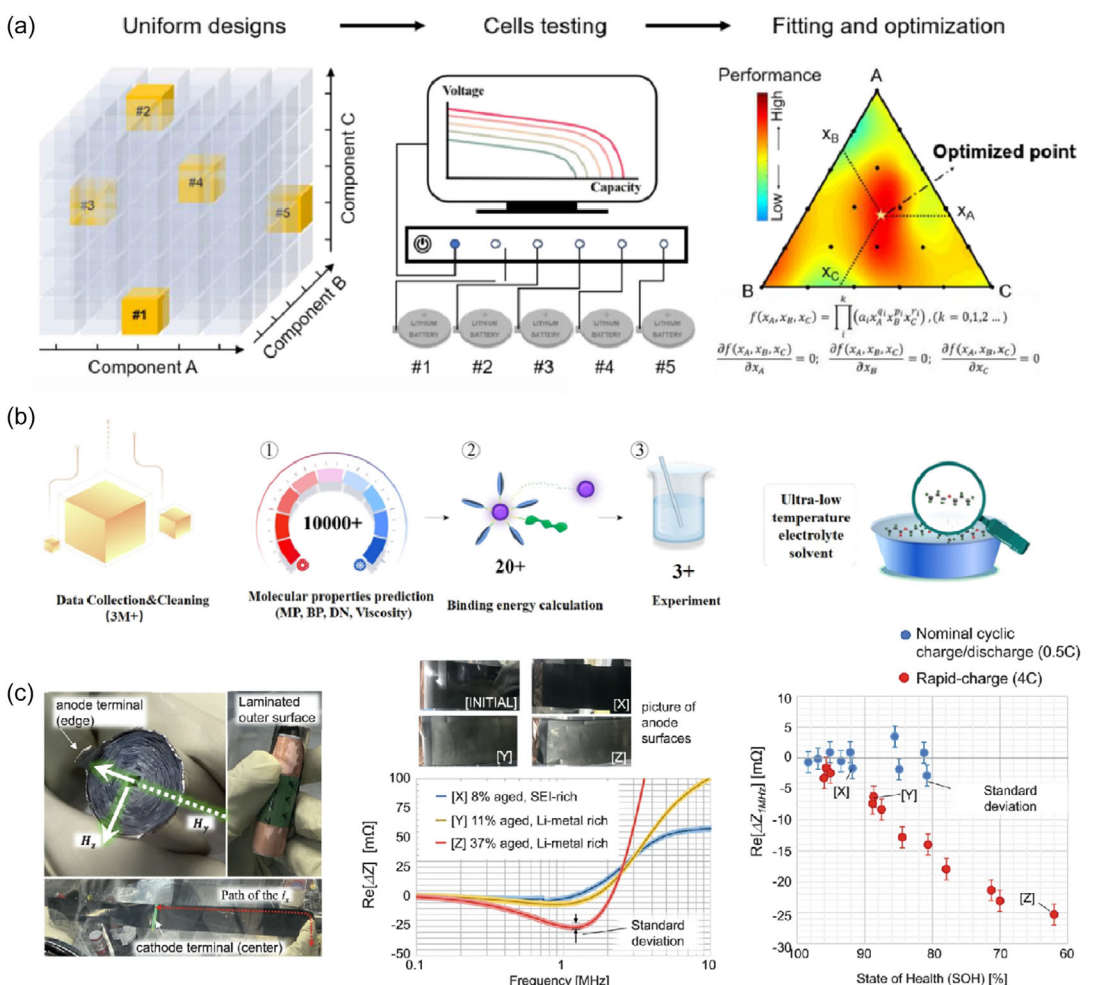


**Figure 10.** a) The implementation process of the unified design method. Reproduced with permission.<sup>[93]</sup> Copyright 2022, Elsevier. b) Schematic diagram of the process for screening electrolyte molecules by combining machine learning and first-principles calculations. Reproduced with permission.<sup>[95]</sup> Copyright 2025 American Chemical Society. c) NDT of lithium metal plating in commercially available batteries. Reproduced with permission.<sup>[102]</sup> Copyright 2023 Nature Publishing Group.

constructing stable electrode-electrolyte interface films, and expanding the electrochemical working window. Despite significant advancements in low-temperature applications, further development of low-temperature electrolytes still faces numerous challenges. 1) Absence of an ideal low-temperature electrolyte system. The currently reported low-temperature electrolytes have indeed enhanced the low-temperature performance of batteries to a certain extent.<sup>[85–87]</sup> However, they still fall short of fully satisfying the stringent demands for low-temperature performance in practical applications. For instance, although some weakly solvated electrolytes can reduce the desolvation energy of Li<sup>+</sup>, the ionic conductivity is also compromised, so the internal resistance is significantly increased.<sup>[88–92]</sup> Therefore, there is highly urgent to develop uniform design guidelines to design ideal low-temperature electrolytes (Figure 10a).<sup>[93]</sup> Moreover, the predominant design strategies for previously reported low-temperature electrolytes are mainly based on a “trial-and-error” method, which is not only time-consuming but also inefficient, posing significant hurdles in efficiently identifying the optimal electrolytes. Artificial intelligence (AI) or machine learning is emerges as an useful tool to facilitate electrolyte design to improve the efficiency of electrolyte screening (Figure 10b).<sup>[94–97]</sup> However, most of AI used in designing ideal electrolytes are still limited to the design of electrolyte via property prediction of solvents, and the optimization of the whole electrolytes should be taken into account in the future. 2) Urgent need for the development of nondestructive (NDT) testing technology. In low-temperature environments, lithium-ion batteries are prone to lithium dendrite growth, which not only degrades battery performance but can also lead to safety issues such as short circuits and thermal runaway.<sup>[14,98–100]</sup> Current characterization techniques, limited by the sealed battery system, can only be performed after the battery is disassembled, leading to errors in detection and nonreal-time monitoring. Therefore, developing NDT technology that can monitor lithium dendrite growth in real time and with high accuracy is of great significance. Developing nondestructive techniques with high spatiotemporal resolution—such as ultrasound, synchrotron X-ray, or fiber-coupled diagnostics enable real-time dendrite early-warning and establish safety thresholds for the next generation low-temperature batteries. Future advancements in NDT technology will significantly contribute to the development of next-generation low-temperature battery technology (Figure 10c).<sup>[101–103]</sup> 3) Limited practical application of low-temperature electrolytes. Previous research has primarily focused on how to enhance the performance of batteries in low-temperature conditions using these electrolytes. Unfortunately, this focus has often overshadowed the critical issues of cost and environmental impact involved in their actual production and use. The reasons behind the observed phenomenon of low-temperature electrolytes exhibiting greater difficulty in charging than discharging at low-temperature remain unclear. Moreover, certain electrolyte formulations, such as high-entropy electrolytes, are plagued by high preparation costs and complex manufacturing processes, which pose significant barriers to their large-scale commercial application. Designing low-cost, high-safety, and environmentally friendly electrolytes is a major challenge to promote the low-temperature performance of LIBs,

but the synergy between electrolytes and electrodes cannot be ignored. Moreover, the development of emerging technologies such as solid-state electrolytes, sodium-ion batteries, and zinc-ion batteries may lead cryogenic batteries to a broader future.<sup>[104–106]</sup>

## Acknowledgements

This work was supported by the National Natural Science Foundation of China (No. 22379164) and the Natural Science Foundation of Hunan Province (2023JJ40662).

## Conflict of Interest

The authors declare no conflict of interest.

## Author Contributions

**Wanyao Zhang:** writing—original draft (lead). **Tao Teng:** conceptualization (equal). **Wenyu Kuang:** data curation (equal). **Di Lu:** methodology (equal); methodology (equal). **Xianxian Shi:** project administration (equal). **Yufang Chen:** project administration (supporting). **Chunman Zheng:** supervision (supporting). **Jilei Liu:** writing—review and editing (equal).

**Keywords:** electrolytes • lithium batteries • lithium dendrites • low-temperature • solvation structure

- [1] M. C. Smart, B. V. Ratnakumar, R. C. Ewell, S. Surampudi, F. J. Puglia, R. Gitzdanner, *Electrochim. Acta* **2018**, *268*, 27.
- [2] D. Hubble, D. E. Brown, Y. Zhao, C. Fang, J. Lau, B. D. McCloskey, G. Liu, *Energy Environ. Sci.* **2022**, *15*, 550.
- [3] M. Li, J. Lu, Z. Chen, K. Amine, *Adv. Mater.* **2018**, *30*, 1800561.
- [4] X. Fan, C. Wang, *Chem. Soc. Rev.* **2021**, *50*, 10486.
- [5] L. Trahey, F. R. Brushett, N. P. Balsara, G. Ceder, L. Cheng, Y.-M. Chiang, N. T. Hahn, B. J. Ingram, S. D. Minteer, J. S. Moore, K. T. Mueller, L. F. Nazar, K. A. Persson, D. J. Siegel, K. Xu, K. R. Zavadil, V. Srinivasan, G. W. Crabtree, *Proc. Natl. Acad. Sci.* **2020**, *117*, 12550.
- [6] T. M. Bandhauer, S. Garimella, T. F. Fuller, *J. Electrochem. Soc.* **2011**, *158*, R1.
- [7] M.-T. F. Rodrigues, G. Babu, H. Gullapalli, K. Kalaga, F. N. Sayed, K. Kato, J. Joyner, P. M. Ajayan, *Nat. Energy* **2017**, *2*, 17108.
- [8] H. Luo, Y. Wang, Y.-H. Feng, X.-Y. Fan, X. Han, P.-F. Wang, *Mater.* **2022**, *15*, 8166.
- [9] N. Zhang, T. Deng, S. Zhang, C. Wang, L. Chen, C. Wang, X. Fan, *Adv. Mater.* **2022**, *34*, e2107899.
- [10] P. Lyu, X. Liu, J. Qu, J. Zhao, Y. Huo, Z. Qu, Z. Rao, *Energy Storage Mater.* **2020**, *31*, 195.
- [11] X. Su, Y. Xu, Y. Wu, H. Li, J. Yang, Y. Liao, R. Qu, Z. Zhang, *Energy Storage Mater.* **2023**, *56*, 642.
- [12] X. Dong, Y.-G. Wang, Y. Xia, *Acc. Chem. Res.* **2021**, *54*, 3883.
- [13] R. Hou, S. Guo, H. Zhou, *Adv. Energy Mater.* **2023**, *13*, 1.
- [14] W. Yu, Z. Xing, W. Ruixi, Z. Tao, X. Peitao, S. Yupeng, X. Yukang, L. Yajie, *Energy Storage Mater.* **2024**, *69*, 103369.
- [15] P. Xiao, Y. Zhao, Z. Piao, B. Li, G. Zhou, H.-M. Cheng, *Energy Environ. Sci.* **2022**, *15*, 2435.
- [16] Y. Huang, C. Wang, H. Lv, Y. Xie, S. Zhou, Y. Ye, E. Zhou, T. Zhu, H. Xie, W. Jiang, X. Wu, X. Kong, H. Jin, H. Ji, *Adv. Mater.* **2023**, *36*, e2308675.
- [17] C. Sun, X. Ji, S. Weng, R. Li, X. Huang, C. Zhu, X. Xiao, T. Deng, L. Fan, L. Chen, X. Wang, C. Wang, X. Fan, *Adv. Mater.* **2022**, *34*, e2206020.
- [18] Y. X. Yao, X. Chen, N. Yao, J. H. Gao, G. Xu, J. F. Ding, C. L. Song, W. L. Cai, C. Yan, Q. Zhang, *Angew. Chem.* **2023**, *62*, e202214828.

- [19] G. Zhu, K. Wen, W. Lv, X. Zhou, Y. Liang, F. Yang, Z. Chen, M. Zou, J. Li, Y. Zhang, W. He, *J. Power Sources* **2015**, *300*, 29.
- [20] S. Tu, B. Zhang, Y. Zhang, Z. Chen, X. Wang, R. Zhan, Y. Ou, W. Wang, X. Liu, X. Duan, L. Wang, Y. Sun, *Nat. Energy* **2023**, *8*, 1365.
- [21] B. Wen, Z. Deng, P.-C. Tsai, Z. W. Lebens-Higgins, L. F. J. Piper, S. P. Ong, Y.-M. Chiang, *Nat. Energy* **2020**, *5*, 578.
- [22] J. Wang, D. Yu, X. Sun, H. Wang, J. Li, *eScience* **2024**, *5*, 70.
- [23] Y. S. Meng, V. Srinivasan, K. Xu, *Science* **2022**, *378*, eabq3750.
- [24] R. Pathak, K. Chen, A. Gurung, K. M. Reza, B. Bahrami, J. Pokharel, A. Baniya, W. He, F. Wu, Y. Zhou, K. Xu, Q. Q. Qiao, *Nat. Commun.* **2020**, *11*, 93.
- [25] Y. Gao, T. Rojas, K. Wang, S. Liu, D. Wang, T. Chen, H. Wang, A. T. Ngo, D. Wang, *Nat. Energy* **2020**, *5*, 534.
- [26] Y. Gao, Z. Yan, J. L. Gray, X. He, D. Wang, T. Chen, Q. Huang, Y. C. Li, H. Wang, S. H. Kim, T. E. Mallouk, D. Wang, *Nat. Mater.* **2019**, *18*, 384.
- [27] Y. Feng, L. Zhou, H. Ma, Z. Wu, Q. Zhao, H. Li, K. Zhang, J. Chen, *Energy Environ. Sci.* **2022**, *15*, 1711.
- [28] J.-G. Zhang, W. Xu, J. Xiao, X. Cao, J. Liu, *Chem. Rev.* **2020**, *120*, 13312.
- [29] X.-B. Cheng, R. Zhang, C.-Z. Zhao, Q. Zhang, *Chem. Rev.* **2017**, *117*, 10403.
- [30] Z. Yu, P. E. Rudnicki, Z. Zhang, Z. Huang, H. Celik, S. T. Oyakhire, Y. Chen, X. Kong, S. C. Kim, X. Xiao, H. Wang, Y. Zheng, G. A. Kamat, M. S. Kim, S. F. Bent, J. Qin, Y. Cui, Z. Bao, *Nat. Energy* **2022**, *7*, 94.
- [31] Z. Yu, H. Wang, X. Kong, W. Huang, Y. Tsao, D. G. Mackanic, K. Wang, X. Wang, W. Huang, S. Choudhury, Y. Zheng, C. V. Amanchukwu, S. T. Hung, Y. Ma, E. G. Lomeli, J. Qin, Y. Cui, Z. Bao, *Nat. Energy* **2020**, *5*, 526.
- [32] C. S. Rustomji, Y. Yang, T. K. Kim, J. Mac, Y. J. Kim, E. Caldwell, H. Chung, Y. S. Meng, *Science* **2017**, *356*, eaal4263.
- [33] T. Li, X.-Q. Zhang, P. Shi, Q. Zhang, *Joule* **2019**, *3*, 2647.
- [34] J. Hou, M. Yang, D. Wang, J. Zhang, *Adv. Energy Mater.* **2020**, *10*, 1.
- [35] Q. Li, Z. Cao, W. Wahyudi, G. Liu, G.-T. Park, L. Cavallo, T. D. Anthopoulos, L. Wang, Y.-K. Sun, H. N. Alshareef, J. Ming, *ACS Energy Lett.* **2020**, *6*, 69.
- [36] Z. Wang, Z. Sun, J. Li, Y. Shi, C. Sun, B. An, H. M. Cheng, F. Li, *Chem. Soc. Rev.* **2021**, *50*, 3178.
- [37] A. C. Thenuwara, P. P. Shetty, M. T. McDowell, *Nano Lett.* **2019**, *19*, 8664.
- [38] X. Fan, X. Ji, L. Chen, J. Chen, T. Deng, F. Han, J. Yue, N. Piao, R. Wang, X. Zhou, X. Xiao, L. Chen, C. Wang, *Nat. Energy* **2019**, *4*, 882.
- [39] J. Holoubek, H. Liu, Z. Wu, Y. Yin, X. Xing, G. Cai, S. Yu, H. Zhou, T. A. Pascal, Z. Chen, P. Liu, *Nat. Energy* **2021**, *6*, 303.
- [40] J. Wang, W. Huang, A. Pei, Y. Li, F. Shi, X. Yu, Y. Cui, *Nat. Energy* **2019**, *4*, 664.
- [41] Y. Yin, Y. Yang, D. Cheng, M. Mayer, J. Holoubek, W. Li, G. Raghavendran, A. Liu, B. Lu, D. M. Davies, Z. Chen, O. Borodin, Y. S. Meng, *Nat. Energy* **2022**, *7*, 548.
- [42] T. D. Pham, A. B. Faheem, S. Y. Chun, J. R. Rho, K. Kwak, K. K. Lee, *Adv. Energy Mater.* **2021**, *11*, 2003520.
- [43] F. Qiu, X. Li, H. Deng, D. Wang, X. Mu, P. He, H. Zhou, *Adv. Energy Mater.* **2018**, *9*, 1803372.
- [44] J. Zheng, M. H. Engelhard, D. Mei, S. Jiao, B. J. Polzin, J.-G. Zhang, W. Xu, *Nat. Energy* **2017**, *2*, 17012.
- [45] Z. Li, Y. Chen, X. Yun, P. Gao, C. Zheng, P. Xiao, *Adv. Funct. Mater.* **2023**, *33*, 202300502.
- [46] B. Roy, P. Cherepanov, C. Nguyen, C. Forsyth, U. Pal, T. C. Mendes, P. Howlett, M. Forsyth, D. MacFarlane, M. Kar, *Adv. Energy Mater.* **2021**, *11*, 2101422.
- [47] H. Zheng, H. Xiang, F. Jiang, Y. Liu, Y. Sun, X. Liang, Y. Feng, Y. Yu, *Adv. Energy Mater.* **2020**, *10*, 2001440.
- [48] R. Weber, M. Genovese, A. J. Louli, S. Hames, C. Martin, I. G. Hill, J. R. Dahn, *Nat. Energy* **2019**, *4*, 683.
- [49] J. Xu, V. Kovarga, A. Phan, A. min Li, N. Zhang, M. Baek, C. Jayawardhana, B. L. Lucht, A. T. Ngo, C. Wang, *Adv. Mater.* **2023**, *36*, 2470049.
- [50] L. Li, W. Lv, J. Chen, C. Zhu, S. Dmytro, Q. Zhang, S. Zhong, *ACS Appl. Energy Mater.* **2022**, *5*, 11900.
- [51] Y. Zhao, Z. Hu, Z. Zhao, X. Chen, S. Zhang, J. Gao, J. Luo, *J. Am. Chem. Soc.* **2023**, *145*, 22184.
- [52] X. Meng, J. Qin, Y. Liu, Z. Liu, Y. Zhao, Z. Song, H. Zhan, *Chem. Eng. J.* **2023**, *465*, 142913.
- [53] L. Che, Z. Hu, T. Zhang, P. Dai, C. Chen, C. Shen, H. Huang, L. Jiao, T. Jin, K. Xie, *Battery Energy* **2024**, *3*, 20230064.
- [54] R. Zhao, Y. Gao, Z. Qin, Y. Li, T. Zhang, A. Pan, N. Zhang, R. Ma, X. Liu, G. Chen, *Adv. Powder Mater.* **2025**, *4*, 100296.
- [55] F. Cheng, W. Zhang, Q. Li, C. Fang, J. Han, Y. Huang, *ACS Nano* **2023**, *17*, 24259.
- [56] Q. Wang, C. Zhao, Z. Yao, J. Wang, F. Wu, S. G. H. Kumar, S. Ganapathy, S. Eustace, X. Bai, B. Li, J. Lu, M. Wagemaker, *Adv. Mater.* **2023**, *35*, e2210677.
- [57] C.-B. Jin, N. Yao, Y. Xiao, J. Xie, *Adv. Mater.* **2023**, *35*, 2208340.
- [58] X. Li, M. Li, Y. Liu, Y. Jie, W. Li, Y. Chen, F. Huang, Y. Zhang, T. M. Sohail, S. Wang, X. Zhu, T. Cheng, M. D. Gu, S. Jiao, R. Cao, *J. Am. Chem. Soc.* **2024**, *146*, 17023.
- [59] R. Gu, D. Zhang, S. Zhu, J. Xu, K. Ding, Q. Gao, Q. Xu, P. Shi, H. Li, Y. Min, *Adv. Funct. Mater.* **2024**, *34*, 1.
- [60] R. Yu, Z. Li, X. Zhang, X. Guo, *Chem. Commun.* **2022**, *58*, 8994.
- [61] Y. Yang, Y. Chen, L. Tan, J. Zhang, N. Li, X. Ji, Y. Zhu, *Angew. Chem. Int. Ed.* **2022**, *61*, e202209619.
- [62] H. Zhang, Z. Zeng, Q. Wu, X. Wang, M. Qin, S. Lei, S. Cheng, J. Xie, *J. Energy Chem.* **2024**, *90*, 380.
- [63] Z. Li, Y.-X. Yao, M. Zheng, S. Sun, Y. Yang, Y. Xiao, L. Xu, C.-B. Jin, X.-Y. Yue, T. Song, P. Wu, C. Yan, Q. Zhang, *Angew. Chem. Int. Ed.* **2024**, *64*, e202409409.
- [64] Y. Chen, Q. He, Y. Zhao, W. Zhou, P. Xiao, P. Gao, N. Tavajohi, J. Tu, B. Li, X. He, L. Xing, X. Fan, J. Liu, *Nat. Commun.* **2023**, *14*, 8326.
- [65] J. Holoubek, M. Yu, S. Yu, M. Li, Z. Wu, D. Xia, P. Bhaladhare, M. S. Gonzalez, T. A. Pascal, P. Liu, Z. Chen, *ACS Energy Lett.* **2020**, *5*, 1438.
- [66] Y. Zou, Z. Ma, G. Liu, Q. Li, D. Yin, X. Shi, Z. Cao, Z. Tian, H. Kim, Y. Guo, C. Sun, L. Cavallo, L. Wang, H. N. Alshareef, Y. K. Sun, J. Ming, *Angew. Chem. Int. Ed.* **2023**, *62*, 1.
- [67] Z. Wang, Z. Sun, Y. Shi, F. Qi, X. Gao, H. Yang, H. M. Cheng, F. Li, *Adv. Energy Mater.* **2021**, *11*, 1.
- [68] J. Liu, B. Yuan, N. He, L. Dong, D. Chen, S. Zhong, Y. Ji, J. Han, C. Yang, Y. Liu, W. He, *Energy Environ. Sci.* **2023**, *16*, 1024.
- [69] Y. Wang, Z. Li, W. Xie, Q. Zhang, Z. Hao, C. Zheng, J. Hou, Y. Lu, Z. Yan, Q. Zhao, J. Chen, *Angew. Chem. Int. Ed.* **2024**, *63*, 1.
- [70] J. Xu, J. Zhang, T. P. Pollard, Q. Li, S. Tan, S. Hou, H. Wan, F. Chen, H. He, E. Hu, K. Xu, X.-Q. Yang, O. Borodin, C. Wang, *Nature* **2023**, *614*, 694.
- [71] D. Lu, R. Li, M. M. Rahman, P. Yu, L. Lv, S. Yang, Y. Huang, C. Sun, S. Zhang, H. Zhang, J. Zhang, X. Xiao, T. Deng, L. Fan, L. Chen, J. Wang, E. Hu, C. Wang, X. Fan, *Nature* **2024**, *627*, 101.
- [72] L. Luo, K. Chen, H. Chen, H. Li, R. Cao, X. Feng, W. Chen, Y. Fang, Y. Cao, *Adv. Mater.* **2023**, *36*, 2308881.
- [73] J. Shi, C. Xu, J. Lai, Z. Li, Y. Zhang, Y. Liu, K. Ding, Y. P. Cai, R. Shang, Q. Zheng, *Angew. Chem. Int. Ed.* **2023**, *62*, e202218151.
- [74] P. Lai, Y. Zhang, B. Huang, X. Deng, H. Hua, Q. Chen, S. Zhao, J. Dai, P. Zhang, J. Zhao, *Energy Storage Mater.* **2024**, *67*, 103314.
- [75] A. Wang, Y. Song, Z. Zhao, X. Li, Z. Hu, J. Luo, *Adv. Funct. Mater.* **2023**, *33*, 2302503.
- [76] X. Yin, B. Li, H. Liu, B. Wen, J. Liu, M. Bai, Y. Zhang, Y. Zhao, X. Cui, Y. Su, G. Gao, S. Ding, W. Yu, *Joule* **2025**, *9*, 101823.
- [77] W. Zhang, H. Xia, Z. Zhu, Z. Lv, S. Cao, J. Wei, Y. Luo, Y. Xiao, L. Liu, X. Chen, *CCS Chem.* **2021**, *3*, 1245.
- [78] B. Nan, L. Chen, N. D. Rodrigo, O. Borodin, N. Piao, J. Xia, T. Pollard, S. Hou, J. Zhang, X. Ji, J. Xu, X. Zhang, L. Ma, X. He, S. Liu, H. Wan, E. Hu, W. Zhang, K. Xu, X. Q. Yang, B. Lucht, C. Wang, *Angew. Chem. Int. Ed.* **2022**, *61*, e202205967.
- [79] L. Liu, Z. Shadike, X. Cai, M. Hong, Y. Gao, S. Shen, J. Zhang, *J. Mater. Chem. A* **2024**, *12*, 6947.
- [80] J. Holoubek, K. Yu, J. Wu, S. Wang, M. Li, H. Gao, Z. Hui, G. Hyun, Y. Yin, A. U. Mu, K. Kim, A. Liu, S. Yu, T. A. Pascal, P. Liu, Z. Chen, *Proc. Natl. Acad. Sci.* **2023**, *120*, e2310714120.
- [81] J. Ming, Z. Cao, Y. Wu, W. Wahyudi, W. Wang, X. Guo, L. Cavallo, J.-Y. Hwang, A. Shamim, L.-J. Li, Y.-K. Sun, H. N. Alshareef, *ACS Energy Lett.* **2019**, *4*, 2613.
- [82] A. C. Thenuwara, P. P. Shetty, N. Kondekar, S. E. Sandoval, K. Cavallaro, R. May, C.-T. Yang, L. E. Marbella, Y. Qi, M. T. McDowell, *ACS Energy Lett.* **2020**, *5*, 2411.
- [83] W. Lv, C. Zhu, J. Chen, C. Ou, Q. Zhang, S. Zhong, *Chem. Eng. J.* **2021**, *418*, 129400.
- [84] W. Zhang, Y. Lu, Q. Feng, H. Wang, G. Cheng, H. Liu, Q. Cao, Z. Luo, P. Zhou, Y. Xia, W. Hou, K. Zhao, C. Du, K. Liu, *Nat. Commun.* **2025**, *16*, 3344.
- [85] Z. Cui, D. Wang, J. Guo, Q. Nian, D. Ruan, J. Fan, J. Ma, L. Li, Q. Dong, X. Luo, Z. Wang, X. Ou, R. Cao, S. Jiao, Y. Ren, *J. Am. Chem. Soc.* **2024**, *146*, 27644.
- [86] S. Yuan, S. Cao, X. Chen, J. Wei, Z. Lv, H. Xia, L. Chen, R. B. F. Ng, F. L. Tan, H. Li, X. J. Loh, S. Li, X. Feng, X. Chen, *J. Am. Chem. Soc.* **2025**, *147*, 4089.
- [87] X. He, Y. Ling, Y. Wu, Y. Lei, D. Cao, C. Zhang, *Small* **2025**, *21*, e2412817.
- [88] Y. Wu, Q. Hu, H. Liang, A. Wang, H. Xu, L. Wang, X. He, *Adv. Energy Mater.* **2023**, *13*, 1.
- [89] T. Qin, H. Yang, L. Wang, W. Xue, N. Yao, Q. Li, X. Chen, X. Yang, X. Yu, Q. Zhang, H. Li, *Angew. Chem.* **2024**, *63*, e202408902.
- [90] Y.-C. Gao, N. Yao, X. Chen, L. Yu, R. Zhang, Q. Zhang, *J. Am. Chem. Soc.* **2023**, *145*, 23764.

- [91] A. Ishikawa, K. Sodeyama, Y. Igarashi, T. Nakayama, Y. Tateyama, M. Okada, *Phys. Chem. Chem. Phys.* **2019**, *21*, 26399.
- [92] K. Sodeyama, Y. Igarashi, T. Nakayama, Y. Tateyama, M. Okada, *Phys. Chem. Chem. Phys.* **2018**, *20*, 22585.
- [93] W. Xue, T. Qin, Q. Li, M. Zan, X. Yu, H. Li, *Energy Storage Mater.* **2022**, *50*, 598.
- [94] Y. Mo, X. Dong, *Next Energy* **2024**, *3*, 100115.
- [95] Z. Li, W. Wang, W. Zhang, Y. Chen, X. Yun, T. Teng, C. Zheng, L. Xu, M. Tang, Y. Zhao, B. Li, J. Liu, P. Xiao, *ACS Nano* **2025**, *19*, 23294.
- [96] Z. Li, Y. Chen, X. Yun, P. Gao, C. Zheng, P. Xiao, *Adv. Funct. Mater.* **2023**, *33*, 2300502.
- [97] P. Xiao, X. Yun, Y. Chen, X. Guo, P. Gao, G. Zhou, C. Zheng, *Chem. Soc. Rev.* **2023**, *52*, 5255.
- [98] S. C. Kim, X. Kong, R. A. Vila, W. Huang, Y. Chen, D. T. Boyle, Z. Yu, H. Wang, Z. Bao, J. Qin, Y. Cui, *J. Am. Chem. Soc.* **2021**, *143*, 10301.
- [99] K. K. Lee, K. Park, H. Lee, Y. Noh, D. Kossowska, K. Kwak, M. Cho, *Nat. Commun.* **2017**, *8*, 14658.
- [100] W. Zhong, J. Tao, Y. Chen, R. G. White, L. Zhang, J. Li, Z. Huang, Y. Lin, *Adv. Powder Mater.* **2024**, *3*, 100184.
- [101] C. Gervillié-Mouravieff, W. Bao, D. A. Steingart, Y. S. Meng, *Nat. Rev. Electr. Eng.* **2024**, *1*, 547.
- [102] M. Ishigaki, K. Ishikawa, T. Usuki, H. Kondo, S. Komagata, T. Sasaki, *Nat. Commun.* **2023**, *14*, 7275.
- [103] Y. Wei, M. Wang, M. Zhang, T. Cai, Y. Huang, M. Xu, *Electrochim. Energy Rev.* **2025**, *8*, 10.
- [104] Y. Cui, Y. Ni, Y. Wang, L. Wang, W. Yang, S. Wu, W. Xie, K. Zhang, Z. Yan, J. Chen, *Adv. Energy Mater.* **2025**, *15*, 2405363.
- [105] Y. Chen, L. Chen, Z. Dong, C. Lou, Z. Han, X. Li, G. Xiao, W. Lv, Y.-B. He, F. Kang, M. Liu, *J. Am. Chem. Soc.* **2025**, *147*, 20431.
- [106] C. Hu, L. Dai, F. Huang, Y. Yang, S. Liang, G. Fang, Q. Zhang, *Angew. Chem. Int. Ed.* **2025**, *64*, e202508584.

Manuscript received: August 1, 2025

Revised manuscript received: September 30, 2025

Version of record online: